Materials Today Bio 31 (2025) 101569

Contents lists available at ScienceDirect

Materials Today Bio

journal homepage: www.journals.elsevier.com/materials-today-bio

An "EVs-in-ECM" mimicking system orchestrates transcription and translation of RUNX1 for in-situ cartilage regeneration

Qi Cheng [a,b,1], Qianping Guo [a,1], Xiaoyu Zhang [a,1], Yuanchen Zhu [a], Chengyuan Liu [a], Huan Wang [a], Caihong Zhu [a], Li Ni [a,*], Bin Li [a,c,**], Huilin Yang [a,***]

[a] Department of Orthopaedic Surgery, Orthopaedic Institute, The First Affiliated Hospital, Suzhou Medical College, Soochow University, Suzhou, Jiangsu, 215006, China
[b] Orthopaedic Department, Xuzhou Central Hospital, No. 199, The Jiefang South Road, Xuzhou, 221009, Jiangsu, China
[c] Medical 3D Printing Center, Orthopedic Institute, Department of Orthopedic Surgery, The First Affiliated Hospital, School of Biology and Basic Medical Sciences, Suzhou Medical College, Soochow University, Suzhou, Jiangsu, 215006, China

ARTICLE INFO

Keywords:
Cartilage repair
CBFβ
Kartogenin
RUNX1
TD-198946

ABSTRACT

The self-repair ability of articular cartilage is limited, which is one of the most difficult diseases to treat clinically. Kartogenin (KGN) induces chondrogenesis by regulating RUNX1 mRNA translation and the small molecule compound TD-198946 (TD) promotes chondrogenic differentiation of mesenchymal stem cells (MSCs) through increasing the transcription of RUNX1 mRNA. GelMA hydrogel and liposomes are respectively similar to the extracellular matrix (ECM) and extracellular vesicles (EVs). So, we developed an "EVs-in-ECM" mimicking system by incorporating GelMA and KGN/TD-loaded liposomes to investigate the repair effects of cartilage defect. First, western-blot, RNA fluorescence in situ hybridization (FISH), cellular immuno-fluorescence, co-immunoprecipitation (CO-IP), and qRT-PCR techniques showed that KGN regulated RUNX1 mRNA expression, and then promote chondrogenic differentiation of MSCs. Second, the role of RUNX1 was amplified by orchestrating RUNX1 transcription and translation through TD-198946 (TD) and KGN respectively, and the synergistic effects of TD and KGN on chondrogenesis of MSCs in vitro were discovered. Finally, an "EVs-in-ECM" mimicking system was designed for in situ cartilage repair. When GelMA loaded with KGN and TD liposomes, the hydrogel (KGN + TD@ GelMA) showed biological functions by the continuously controlled release of KGN and TD while maintaining its porous structure and mechanical strength, which enhanced the chondrogenesis of MSCs in one system. The repair performance of "EVs-in-ECM" in vivo was assessed using the articular osteochondral defect model of rat. The implantation of KGN + TD@ GelMA hydrogels effectively exerted favorable osteochondral repair effects showing structures similar to the native tissue, and prevented chondrocyte hypertrophy. The study indicate that the "EVs-in-ECM" mimicking system can act as a highly efficient and potent scaffold for osteochondral defect regeneration.

1. Introduction

Osteochondral defects caused by trauma, necrosis, inflammation, and degeneration are some common orthopedic diseases resulting in significant pain and disability [1]. Cartilage regeneration following injury remains a great challenge clinically, which suffers from its avascularity and poor proliferative ability to restrict its spontaneous regeneration. Nowadays, several clinical management methods for cartilage repair, including allografts, mosaicplasty (MO), and autologous chondrocyte implantation (ACI), are limited by disease transmission, fibrocartilage repair, immunogenic rejection, and mechanical inferiority [2,3]. To overcome these limitations, tissue engineering using effective chondrogenesis of mesenchymal stem cells (MSCs) is considered as a favorable alternative to cartilage repair.

Runt-related transcription factor 1 (RUNX1) is a main regulator of articular cartilage homeostasis, which acts by the signaling pathways of

* Corresponding author.
** Corresponding author. Department of Orthopaedic Surgery, Orthopaedic Institute, The First Affiliated Hospital, Suzhou Medical College, Soochow University, Suzhou, Jiangsu, 215006, China.
*** Corresponding author.
E-mail addresses: nili@suda.edu.cn (L. Ni), binli@suda.edu.cn (B. Li), suzhouspine@163.com (H. Yang).
[1] These authors equally contributed to this study.

https://doi.org/10.1016/j.mtbio.2025.101569
Received 4 December 2024; Received in revised form 6 February 2025; Accepted 8 February 2025
Available online 14 February 2025

TGF-β signaling and Wnt signaling in the formation of articular cartilage and osteoarthritis (OA) [4–7]. Increased levels of RUNX1 in MSCs have been demonstrated to stimulate the development of chondrocytes. RUNX1 can effectively promote the expression of chondrogenic transcription factors SOX9 and further enhance cartilage matrix production through interactions with SOX9 [8,9]. Soung et al. [10] have revealed that the gradual loss of RUNX1 function induces a reduction of SOX9 and a delay in the chondrocyte differentiation process. Zhang et al. [4] verified that the deficiency of RUNX1 could facilitate cartilage ossification and osteophyte formation by activating the Wnt pathway. Moreover, the lack of RUNX1 can impede the nuclear translocation of YAP, reducing their ability to interact with RUNX1 in the nucleus, which hinders the expression of target genes like type II collagen(Col II) and SOX9,ultimately worsening cartilage loss [11]. In vivo, Zhou et al. [12] found that the knockout of RUNX1 aggravated cartilage destruction by accelerating the loss of proteoglycan and Col II in the early stage of OA. However, RUNX1 was overexpressed in articular cartilage through adeno-associated virus (AAV). Its protective effect was identified by decelerating the destruction of cartilage during the early stage of OA. Therefore, focusing on RUNX1 may be a successful treatment way for repairing cartilage.

The recent research results have demonstrated that the combination of MSCs with cartilage induced growth factor kartogenin (KGN) provides a promising alternative for repairing injured cartilage [13–15]. However, the mechanism through which KGN regulates the development of cartilage and bone is still unclear. The currently accepted mechanism involves KGN binding to the intracellular protein filamin A (FLNA),leading to the disruption of its interaction with the core-binding factor beta subunit(CBFβ) [16]. CBFβ is a subunit of the CBF family of heterodimeric transcription factors and is crucial in skeletal development by interacting with the CBFα subunits (RUNX1) in the nucleus and enhances the RUNX1-dependent chondrogenesis transcription activity [17]. However, the RUNX1 protein containing a nuclear localization sequence is found only in the nuclei of most cells and tissues, while CBFβ lacking a nuclear localization sequence is unable to autonomously enter the nucleus and is primarily situated in the cytoplasm [18]. This suggests a spatial barrier in the interaction between RUNX1 and CBFβ and reveals unidentified mechanisms through which KGN causes CBFβ to regulate RUNX1. Many studies suggest that CBFβ may be important in the expression of RUNX1, in addition to improving the transcriptional activity of RUNX1. Yan et al. [15] reported that KGN showed little effect on the mRNA level of RUNX1 in MSCs. The in vivo study exhibited that RUNX1 was barely found in the CBFβ−/− mouse [19]. Recent research has shown that eukaryotic translation initiation factor eIF4B may act as a bridging factor for CBFβ to stimulate the attachment of RUNX1 mRNA in the cytoplasm, which is proposed to facilitate translation [17,20]. Thus, this study aims to clarify the role of CBFβ in chondrogenesis and uncover its involvement in regulating RUNX1 translation following KGN treatment.

Though KGN is accepted as an effective drug in cartilage repair, the efficiency is low, and side-effects of KGN are still non-negligible [3,15]. Considering the significant roles of RUNX1 in cartilage regeneration and repair,as well as the involvement of CBFβ in the post-transcriptional translation of RUNX1, the study investigated the potential of certain drugs to enhance RUNX1 mRNA expression in stem cells. Furthermore, the synergistic effect of co-treating with KGN was evaluated to determine if it could increase RUNX1 protein expression by the transcription and translation, thereby enhancing the potential of KGN in promoting chondrogenesis. TD-198946 (TD) is another small molecule promoting chondrogenesis of several stem cells by regulating transcription of RUNX1 mRNA [21]. It has been reported to effectively induce the production of glycosaminoglycan (GAG) and Col II from chondrocytes without promoting endochondral ossification or hypertrophy [22]. Therefore, TD might be a candidate for amplifying the cartilage regeneration effect of KGN by orchestrating RUNX1 transcription in cartilage repair.

The extracellular matrix (ECM) is crucial for providing the requisite microenvironment for the proper regeneration of cartilage tissue [23]. Extracellular vesicles (EVs), which are small particles derived from the plasma membrane and released into the extracellular space by nearly all cell types, are regarded as one of the structural and functional components of the ECM. Recently, EVs have attracted more attention due to their ability to carry nucleic acids, proteins, lipids, and signaling molecules and transfer these contents to target cells [24]. In the development of biomaterial scaffolds, gelatin methacrylate (GelMA) shares comparable characteristics with ECM and supports the proliferation and differentiation of MSCs or chondrocytes. Thus, the recent researches have shown that the hydrogels in combination with growth factors have extensive applications in cartilage tissue engineering [25–27]. However, KGN and TD are both hydrophobic drugs whose application in GelMA might be restricted by their poor aqueous solubility, low drug loading efficiency, and rapid diffusion [28–30]. Liposomes are a preferred choice for KGN and TD loading due to they are similar with EVs in function to protect and transport protein or small molecule effectively [31,32]. Considering the above rationale, an “EVs-in-ECM” mimicking system with controlled release of KGN and TD stimulating RUNX1 transcription and translation for cartilage repair is hereby presented. A phospholipid- and cholesterol-based liposome was utilized to load the bioactive drugs KGN (KGN@Lipo) and TD (TD@Lipo), and further embeded in GelMA hydrogel. Subsequently, the characterization of an “EVs-in-ECM” mimicking system and the synergistic effect of TD and KGN in cartilage repair and subchondral bone reconstruction were investigated in a full-thickness rat knee cartilage defect.

In this work, the function of KGN in the chondrogenesis of MSCs as well as the combined effects of KGN and TD on the in-vitro chondrogenesis of MSCs by regulating RUNX1 transcription and translation were explored, and the mechanism on how KGN targeted CBFβ to regulate the expression of RUNX1 was revealed. Then, an “EVs-in-ECM” mimicking system was established by encapsulating KGN and TD, and the effect of this system on the treatment of MSCs for in-vivo cartilage defects was assessed. It was proposed that the hydrogel loaded with KGN and TD liposomes could facilitate in-situ cartilage repair within a one-step surgical operation by promoting the chondrogenesis of MSCs (Scheme 1).

2. Materials and methods

2.1. Materials

GelMA(EFL-GM-60) and LAP were acquired from Suzhou Intelligent Manufacturing Research Institute in Suzhou, China. Toluidine blue, Safranine O, dexamethasone, insulin-transferrin-sodium selenite, L-proline, ascorbate-2-phosphate, and sodium pyruvate were all acquired from Sigma-Aldrich (St Louis, MO, USA). Cycloheximide(CHX) and MG132 were acquired from MedChemExpress (USA),while KGN and TD were sourced from the same supplier. The eIF4B antibody was purchased from Novus Biologicals (USA). The particulars of other reagents are provided in the experimental methods.

2.2. Cells culture

MSCs were collected from 6-week-old male Sprague-Dawley rats. The cells were kept in an incubator where the temperature was maintained steadily at 37 °C, with constant humidity and a 5 % CO_2 atmosphere. The growth medium for MSCs was refreshed every three days. For all experimental procedures, third-passage MSCs were utilized.

2.3. MSCs differentiation

For the differentiation experiments, MSCs were seeded in 24-well plates at a density of 5×10^4 per well and cultured in the incomplete chondrogenic differentiation medium lacking TGF-β1, with various concentrations (10 nM–1 μM) of KGN, or TD (10 nM–1 μM) + 100 nM

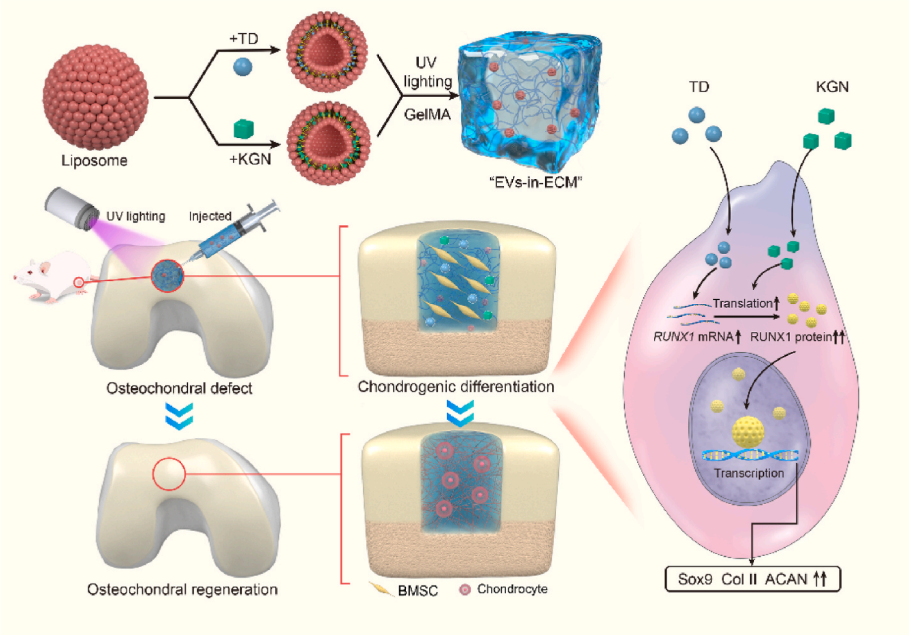

Scheme 1. Schematic diagram of the construction of an "EVs-in-ECM" mimicking system containing KGN@Lipo, TD@Lipo, and GelMA for osteochondral defect repair.

KGN group. The chondrogenic medium was composed of 50 mg/mL insulin-transferrin-selenium, 100 mg/L sodium pyruvate, 50 mg/L ascorbate-2-phosphate, 40 mg/L L-proline, and 100 nM dexamethasone [33,34]. Following one week of incubation, the cells were treated with paraformaldehyde for fixation and subsequently analyzed using Toluidine blue and Safranine O staining.

2.4. Western blot analysis

The MSCs were cultured in 6-well plates and exposed to KGN, TD, or a combination of KGN and TD for either one or seven days in order to assess their potential for chondrogenic differentiation. The RIPA buffer from Beyotime (China) was employed for cell lysis under low-temperature conditions. In particular experiments, nuclear proteins were extracted using a specialized kit for Nuclear Protein Extraction (Beyotime, China). The protein levels were measured utilizing a BCA protein assay kit (Beyotime, China). Before undergoing electrophoresis, the proteins were combined with loading buffer and heated to ensure denaturation. The samples were loaded and separated using SDS-PAGE gels, either 10 % or 15 % (Beyotime, China). The proteins were then transferred onto polyvinylidene fluoride (PVDF) membranes (Beyotime, China). These membranes were then blocked with 5 % bovine serum albumin (BSA) in TBST for half an hour and later incubated with primary antibodies for RUNX1 antibody (ab229482, Abcam, UK); CBFβ antibody (ab133600, Abcam, UK); Col II antibody (ab34712, Abcam, UK); Aggrecan (ACAN) antibody (ab3778, Abcam, UK); SOX9 antibody (ab185230, Abcam, UK); Col X antibody (ab182563, Abcam, UK); H3 antibody (10265-1-AP, Proteintech, UK) and GAPDH antibody (A190156, Abclonal, China) overnight at 4 °C. The membranes were subsequently incubated for 2 h with HRP-conjugated secondary antibodies against rabbit or mouse IgG(H + L) (Beyotime, China). Following washing, signals were detected by an enhanced chemiluminescence system (ECL, Bio-Rad, USA) detection system.

The MSCs were seeded into each well of 6-well plates. After 24 h,the cells were exposed to 100 nM KGN. The culture system was supplemented with CHX(10 μg/mL),a protein synthesis inhibitor,and MG132 (10 μmol/L),a proteasome inhibitor. Subsequently,the expression of RUNX1 was assessed using western blot analysis.

2.5. Quantitative real-time PCR

The MSCs were seeded into 6-well plates, with three replicates being set up for each group. Once the cells had been collected, the total RNA was extracted using a commercial kit (Vazyme, China). The concentration and purity of the RNA were assessed with the NanoDrop 2000 spectrophotometers (Thermo Fisher Scientific, USA). All polymerase chain reaction (PCR) analyses were performed on the CFX96 Real-time system (Bio-Rad, USA), and the gene expression levels were measured with SYBR Green Master (Bio-Rad, USA) according to the manufacturer's instructions. The genes and their corresponding primers are listed in Table S1 of the Supporting Information. The relative gene levels was normalized to the housekeeping gene GAPDH and analyzed by the $2^{-\Delta\Delta Ct}$ method.

2.6. Plasmid transfection and Co-immunoprecipitation

All HA-tagged CBFβ plasmids were generated and their sequencing was verified by GenePharma (Shanghai, China). The cells were plated in 6-well culture dishes and transfected at 80 % density using LipofectamineTM3000 transfection reagent, following the manufacturer's instructions from Thermofisher,USA. First, the medium was changed with serum-free DMEM. Next, the HA-tagged CBFβ (2, 3, 4 μg) and the empty plasmids were individually combined with 5 μL of P3000TM Reagent in 125 μL serum-free DMEM for 5 min, while 5 μL lipo3000 was mixed with 125 μL serum-free DMEM for 5 min. The plasmids solution was mixed with lipo3000 solution for 20 min, then added to the cells. The cell medium was changed to DMEM with 10 % serum after 6 h. Transfection efficiency was assessed through immunofluorescence and western blot after 48 h.

Co-IP was performed according to the protocol of Co-immunoprecipitation Kit (Med ChemExpress, USA). Following 6 h of transfection, the medium was removed and replaced with DMEM with 10 % serum cultured for 48 h, followed by combination with or without 100 nM KGN for 24 h. The Protein A/G Magnetic Beads were mixed with HA antibody (Proteintech, USA) or IgG antibody (Proteintech, USA) and incubated at room temperature for 30 min. The MSCs lysates were incubated with the Protein A/G Magnetic Beads, which were bound to the antibody against HA or IgG, followed by rotation for 2 h at 4 °C. The

magnetic beads were then collected by magnetic separator. All proteins that were not specifically bound were eliminated with washing buffer. The bounded proteins HA-CBFβ and eIF4B were eluted from the beads with SDS-PAGE loading buffer for 10 min at 95 °C, then followed by western blotting analysis.

2.7. Immunofluorescence

The cells attached to glass cover slips were treated with 4 % paraformaldehyde for fixation, followed by permeabilization with 0.1 % Triton X-100 (Sigma-Aldrich, USA) for 10 min. Blocking was performed with 1 % BSA over a period of 30 min, followed by an overnight incubation with primary antibody Col II, ACAN, RUNX1, eIF4B and CBFβ (sc-56751, Santa Cruz; ab133600, Abcam) at a dilution of 1:200. After washing three times with PBS,the cells were exposed to Alexa Fluor® 647 or 488 conjugated secondary antibodies (Abcam, USA) for 1 h. The cell nuclei were subsequently stained using DAPI (Beyotime, China). Fluorescence microscopy was used to capture the images of the stained cells.

2.8. RNA fluorescence in situ hybridization

The fluorescence in situ Hybridization (FISH) assay was carried out on MSCs. GenePharma (Shanghai, China) designed and synthesized Cy3-labeled RUNX1 mRNA probes (Table S2) for the FISH assay. The hybridization was carried out using a FISH kit accordance to the manufacturer's instructions. After conducting in situ hybridization,the samples were subsequently blocked for 1 h in 1 % BSA. Subsequently, samples were incubated with the primary antibody anti-CBFβ (1:200) overnight at 4 °C; washed three times with 1 × PBS; and incubated with the secondary antibody Anti-Rabbit IgG (H + L) for 1 h. DAPI was used for nuclear staining. Images were captured using fluorescence microscopy.

2.9. The "EVs-in-ECM" mimicking system preparation and characterization

The liposomes were fabricated using the thin-film dispersion method according to the previous report [30]. First, 3 mg KGN or TD, 80 mg lecithin, and 20 mg cholesterol were fully dissolved in 30 mL of chloroform. Then, the mixed solution was placed in a rotary vacuum evaporator at a speed of 100 r/min and 35 °C for 30 min to remove the chloroform and generate a thin lipid film. Then, 5 mL of phosphate buffer saline (PBS) was added to hydrate the lipid film. The liposomal pellet was washed and filtered to remove impurities. The fabrication of Liposomes/GelMA composite hydrogels was carried out by incorporating liposomes into a 5 % w/v GelMA solution that contained 0.25 % LAP. Subsequently, the mixture was irradiated with a UV light having a wavelength of 405 nm for a duration of 1 min.

The diameter of the liposome was evaluated at 25 °C through the application of dynamic light scattering (DLS) technology, utilizing the NanoBrook Omni particle size analyzer provided by Brookhaven Instruments. The cryo-TEM images were taken with the JEM-2100 LaB6 TEM (JEOL) at the Advanced Imaging and Microscopy Laboratory located within the Maryland Nano Center. The freeze-dried Liposomes/GelMA composite hydrogels were examined for their morphologies by utilizing scanning electron microscopy (SEM, S-4800, Hitachi, Kyoto, Japan).

2.10. Swelling behaviors of an "EVs-in-ECM" mimicking system

The swelling properties of all hydrogels were evaluated following a previous study [35]. Hydrogels with varying solid contents were submerged in PBS at a temperature of 37 °C. At the predetermined interval time points, the hydrogels were taken out from the PBS and their weights were measured after the surface water was removed. The measured weight was noted as Wt, while the initial weight of the hydrogels was recorded as W0. The swelling ratio (SR) was computed in accordance with the following formula: $SR = (Wt-W0)/W0 \times 100\ \%$.

2.11. In vitro drug release of an "EVs-in-ECM" mimicking system

The release curves of KGN@lipo and TD@lipo from the composite hydrogels were investigated to establish their respective release kinetics. Each drug-infused composite hydrogel was submerged in PBS at a temperature of 37 °C and agitated at a speed of 100 revolutions per minute to simulate in vitro release. The release medium was exchanged with fresh PBS at scheduled time intervals, and the NanoDrop 2000 spectrophotometers from Thermo Fisher Scientific in the USA were employed to measure the concentration of the released drugs.

2.12. Degradation rate

The dry scaffolds were measured for their weight, which was recorded as M0. Subsequently, they were immersed in PBS for a period of 50 days at a temperature of 37 °C. At the pre-established time points, the scaffolds were taken out, dried at 60 °C for 4 h, and then their weights were measured and recorded as Mt. The degradation rate was calculated in the following manner: $Mt/M0 \times 100\ \%$.

2.13. Cell culture on hydrogels

MSCs were harvested and subsequently seeded directly onto various liposomes/GelMA composite hydrogels, followed by chondrogenic induction culture for a period of 7 days. Toluidine blue and Safranine O staining were used to assess the successful induction of chondrogenesis.

2.14. In vitro biocompatibility of hydrogels

The assessment of cell morphology was carried out by seeding 2×10^4 cells onto hydrogels placed in 24-well plates and then culturing them for three days. Then, the F-actin of the samples was stained with phalloidin-Rhodamine (Beyotime, China) for 40 min, and the nucleus was stained with DAPI for 10 min. Finally, images were taken by means of fluorescence microscopy. The assessment of cell viability was conducted by employing a Cell Counting Kit-8 sourced from Kumamoto, Japan. 2×10^4 MSCs were seeded in the lower chamber of a 24-well transwell plate, while different hydrogels were positioned in the upper chamber. The cells were incubated on the first, third, and fifth days for 1 h with a 10 % CCK-8 solution at a temperature of 37 °C, then measured at 450 nm.

MSCs were seeded on different hydrogels within a 24-well plate and then incubated for three days with cell culture medium at 37 °C. Subsequently, the cell-seeded hydrogel was incubated with 200 μL working solution of the Calcein-AM/PI Double Staining Kit (Invitrogen, USA) at 37 °C for 15 min. The cells were then observed and images were captured by means of fluorescence microscopy.

2.15. The repairing effects on osteochondral defects

All animal studies were performed in accordance with the Public Health Service policies and the Animal Welfare Act, and were authorized by the Institutional Animal Care and Use Committee of Soochow University (SUDA20231211A04). Seventy-two male Sprague-Dawley rats, aged eight weeks, were divided into six groups with six animals each: (1) sham group (the joint capsule was exposed, and the wound was sutured after reduction of the patella immediately after dislocation); (2) defect group(defect washed with normal saline and wound sutured); (3) GelMA group (injection of 20 μL GelMA solution), (4) KGN@GelMA group (injection of 20 μL KGN@GelMA solution), (5) TD@GelMA group (injection of 20 μL TD@GelMA solution), (6) KGN + TD@GelMA group (injection of 20 μL KGN + TD@GelMA solution). Critical size volumetric

bilateral femur defects sized 2 mm × 2 mm (diameter × height) were created on the trochlea of the distal femur and rinsed with 0.9 % saline.

2.16. Macroscopic assessment, μ-CT, and histological evaluation

Initially, images of the osteochondral defects were taken using a camera. Three experts independently assessed the efficacy of cartilage repairs using the macroscopic evaluation criteria established by the International Cartilage Repair Society (ICRS). The evaluation included the extent of defect filling, integration with adjacent cartilage, visual quality of the repair, and an overall assessment of the repair work [36]. Next, the samples were examined with a μ-CT scanner (SkyScan 1176, SkyScan, Aartselaar, Belgium) to evaluate the reconstruction of the subchondral bone, with a focus on parameters such as bone volume fraction (BVF), trabecular thickness (Tb.Th), and bone mineral density (BMD) within the specified area of interest. The decalcified samples were embedded in paraffin for histological studies, and then thinly sliced into 5 mm sections using a microtome (LE-ICA, SM2000R). Then, the specimens were stained with hematoxylin and eosin (H&E) for histological observation and Safranine O-fast green staining (SO/FG) for distinguishing normal cartilage from bone tissue. Three independent observers scored cartilage using modified O'Driscoll grading system (MODS). Additional sections underwent immunohistochemical analysis. The deparaffinized tissue sections were treated with citric acid for antigen retrieval, followed by incubation with primary antibodies against Col II (1:150 dilution)and Col X (1:150 dilution), and visualization using the HRP/DAB kit from Abcam, UK. The sections were additionally stained with Mayer's hematoxylin. The Image J software was used to quantitatively evaluate the percentage of positive cells.

2.17. Statistical analysis

The data are presented in the form of mean ± standard deviation (SD). For analyzing the differences between two groups, Student's *t*-test was employed when the data followed a normal distribution, and the Mann–Whitney test was utilized for data that did not conform to a normal distribution. In the case of comparisons involving more than two groups, for data with a normal distribution, one-way analysis of variance (ANOVA) was carried out followed by Tukey's multiple comparison test. Meanwhile, for data not adhering to a normal distribution, the post hoc test with Dunnett's T3 was used for assessment. A significant difference is denoted as *($p < 0.05$).

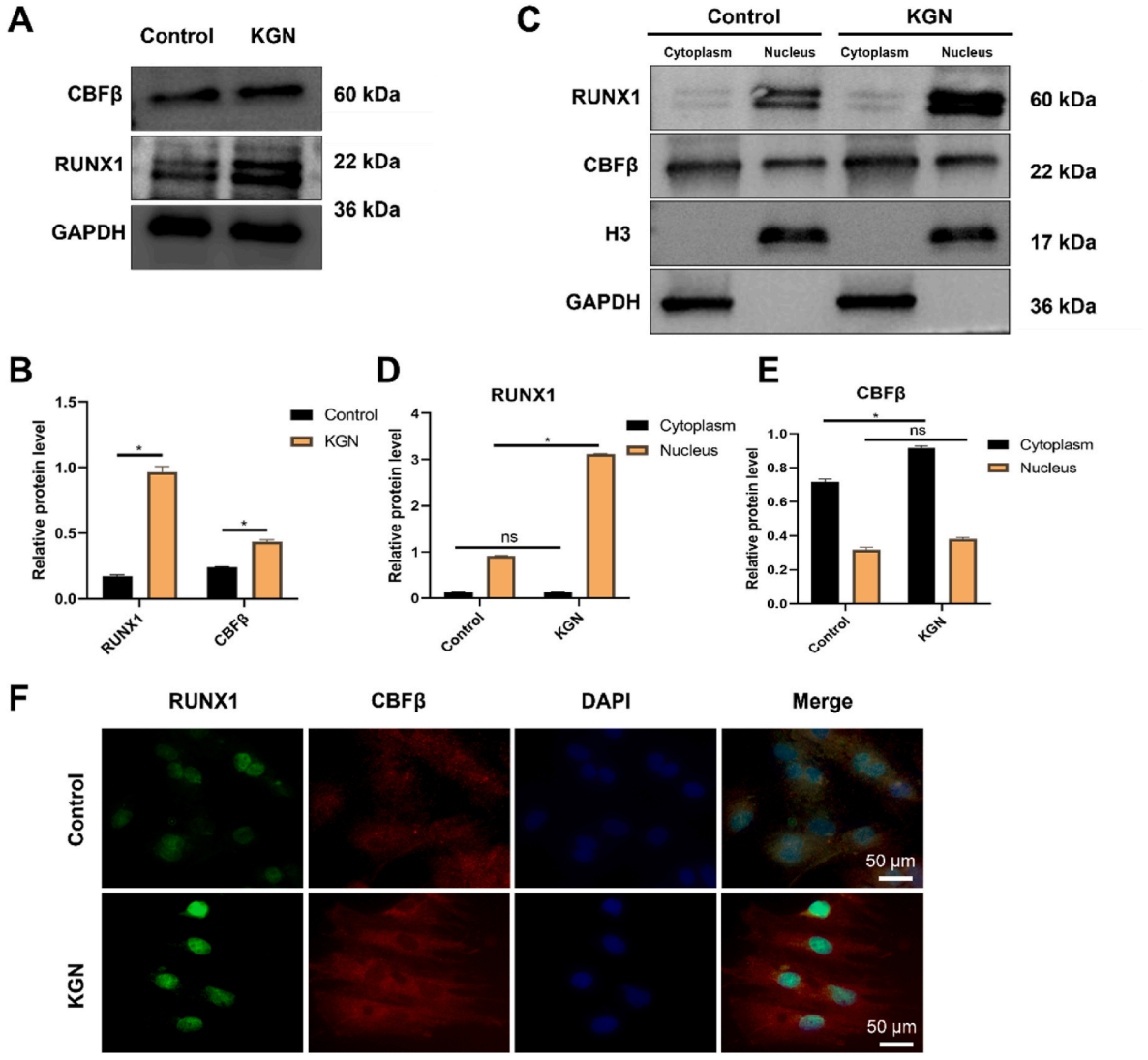

Fig. 1. KGN regulates CBFβ and RUNX1 of MSCs. **(A–B)**. The levels of RUNX1 and CBFβ expression after 24 h of KGN intervention were assessed by western blot analysis. The protein levels were measured using Image J and normalized to GAPDH. **(C–E)**. Protein levels of RUNX1 and CBFβ in the cytoplasm and nucleus were measured after KGN treatment for 24 h. The protein levels were measured using Image J and normalized to GAPDH. **F**. Immuno-fluorescence staining images of MSCs after 24-h KGN intervention; red (CBFβ), green (RUNX1), and blue (nuclei). Scale bar: 50 μm. (n = 3, *: $p < 0.05$; ns: no significant difference).

3. Results

3.1. KGN regulates CBFβ and RUNX1 of MSCs

Initially, two dimensional cultures of MSCs were performed with supplementation of 10 nM to 1 μM KGN for seven days to select the optimal drug concentration (Fig. S1). At the 100 nM concentration, exposure to KGN led to the chondrogenesis of MSCs in vitro, which appeared as strongly stained by Toluidine blue. To explore the effect of KGN on the expression of RUNX1, cells were treated with KGN at a concentration of 100 nM for 12 and 24 h (Fig. S2). Immunofluorescence analysis showed that more RUNX1 proteins were detected in MSCs treated with KGN than those in control-treated MSCs at 24 h. Western blot was further employed to investigate the protein expression of RUNX1 and CBFβ under the identical cell culture conditions. The RUNX1 and CBFβ protein expression was significantly upregulated upon treatment with KGN for 24 h (Fig. 1A–B). After the separation of nuclear and cytoplasmic proteins, western blot analysis was conducted once more. The results indicated that, compared with the control group, there was an evident increase in the CBFβ protein within the cytoplasm and the RUNX1 protein within the nucleus in the KGN group. No obvious upregulation of CBFβ expression was observed in the KGN group in the nucleus (Fig. 1C–E). For the purpose of evaluating the subcellular localization of RUNX1 and CBFβ more directly, cell immunofluorescence staining of RUNX1 and CBFβ was performed. The findings showed that CBFβ and RUNX1 were localized in different cellular compartments, with CBFβ predominantly found in the cytoplasm and RUNX1 mainly presented in the nucleus. However, KGN intervention did not show translocation of CBFβ into the nucleus and binding to RUNX1 (Fig. 1F). Moreover, qRT-PCR analysis showed that, compared with the control group, the mRNA level of RUNX1 in the KGN group had no significant alteration (Fig. S3). These results indicated that although KGN did not influence the transcription level of RUNX1, it might regulate the expression of RUNX1 at the translational level.

3.2. CBFβ regulates RUNX1 mRNA translation via eIF4B

The interaction between the translation initiation factor eIF4B and

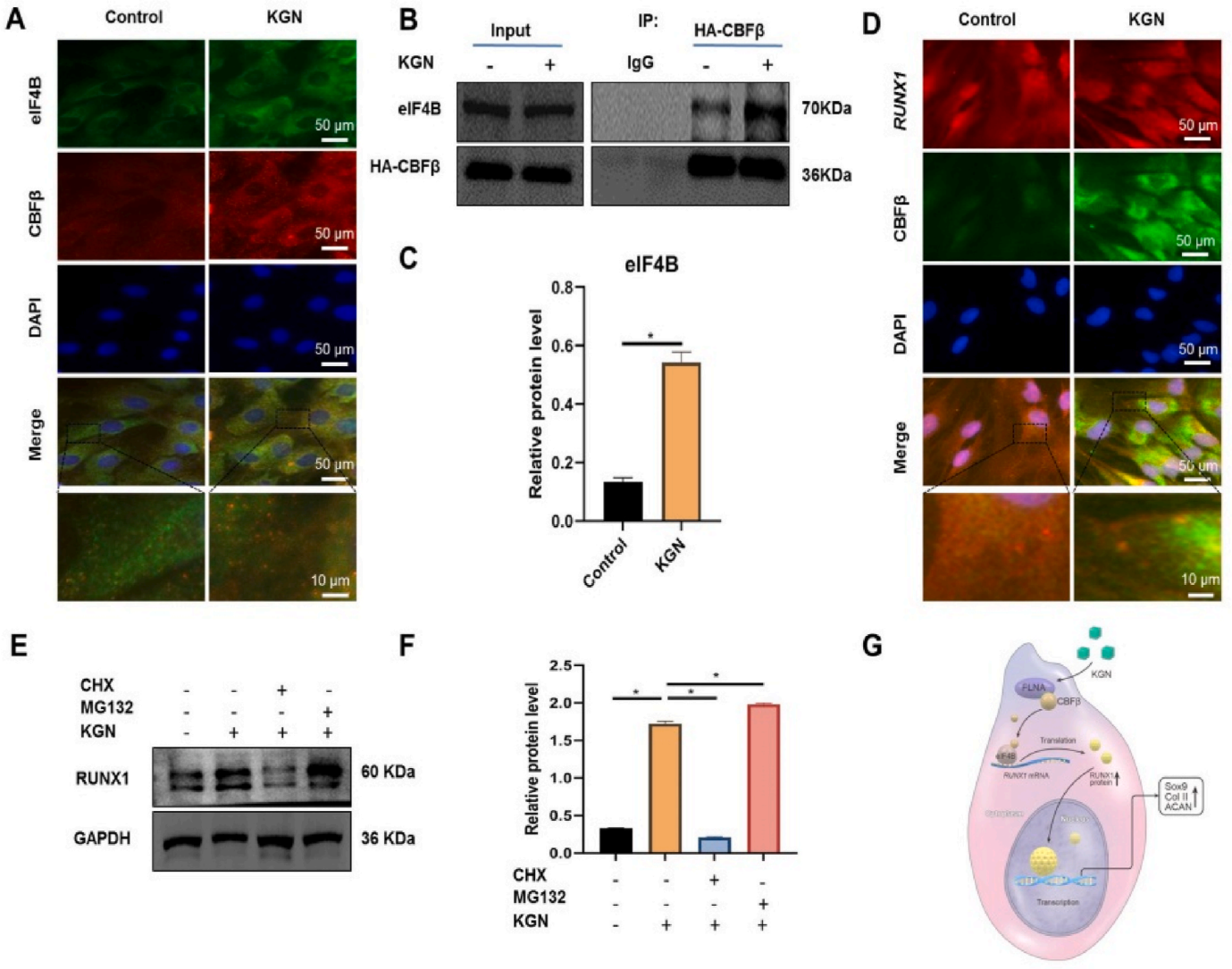

Fig. 2. CBFβ regulates RUNX1 mRNA translation via eIF4B. **A** An immunofluorescence double staining of eIF4B(green), CBFβ(red), and nuclei(blue) was conducted on MSCs cultured with KGN for 24 h. Scale bar: 50 μm. (**B-C**) Co-IP assay and western blot analysis reveal the interaction between CBFβ and eIF4B with 24 h treatment of KGN. The levels of the indicated proteins were quantified by Image J and normalized to HA-CBFβ**. D** Fluorescence in situ hybridization (FISH) (RUNX1)-IF (CBFβ) staining in the MSCs after 24 h. Scale bar: 50 μm. (**E-F**) MSCs treated with KGN and incubated with CHX or MG132 for 24 h. RUNX1 protein amounts were assessed by immunoblot. The levels of indicated proteins were quantitated by Image J and normalized to GAPDH**. G** Schematic model of KGN regulating MSCs differentiation by regulating RUNX1 mRNA translation. (n = 3, *: $p < 0.05$; ns: no significant difference).

CBFβ was investigated to determine whether KGN can regulate the translation of RUNX1 by CBFβ. The localization of eIF4B and CBFβ was visualized using fluorescence microscopy, in which the proteins were observed with the point structure distribution and colocalization was marked in the cytoplasm, and KGN treatment was confirmed to enhance the co-localized expression of CBFβ and eIF4B (Fig. 2A). To further confirm that KGN promotes the binding of CBFβ and eIF4B, transfection and Co-IP experiments were performed. MSCs were transfected with pcDNA3.1 plasmids containing HA-tagged CBFβ, resulting in a significant increase of CBFβ expression observed via immunofluorescence and western blot analysis when the transfected plasmid dosage was 4 μg (Fig. S4). Then, the HA-tagged CBFβ plasmid was transfected into MSCs to perform reciprocal Co-IP experiments treated with or without KGN. The result showed that KGN could enhance the interaction between HA-tagged CBFβ and endogenous eIF4B (Fig. 2B–C). The above results consistently proved the effect of KGN on the interactions of CBFβ and eIF4B in MSCs. Furthermore, immunofluorescence (CBFβ)-FISH (RUNX1) staining revealed the increased CBFβ aggregation of cytoplasm in response to KGN stimulation and the co-localization of CBFβ and RUNX1 mRNA (Fig. 2D). Thus, it is postulated that the interaction between CBFβ and eIF4B is crucial for the translation of RUNX1 mRNA. The stability of RUNX1 was further assessed using protein synthesis inhibitor-CHX and the proteasome inhibitor MG-132 in KGN treatment. Immunoblot suggested that the expression of RUNX1 was significantly inhibited and reduced by CHX, indicating that CBFβ and eIF4B cooperatively enhance RUNX1 translation. Additionally, RUNX1 protein level reduction was alleviated by the proteasome inhibitor MG-132, suggesting that CBFβ is also essential for RUNX1 stability (Fig. 2E–F). Thus, CBFβ and eIF4B are crucial in RUNX1 translation regulation (Fig. 2G).

3.3. Synergistic effects of KGN and TD on chondrogenesis of MSCs

Since KGN can significantly promote the translation of RUNX1, the hypothesis of whether KGN combined with the inducible factor, which increases the transcription level of RUNX1, can synergistically enhance the expression of RUNX1 at the level of transcription and translation, and effectively promote the chondrogenesis of MSCs. TD has been reported to efficiently induce chondrogenic differentiation by enhancing transcription of RUNX1 mRNA [22]. Therefore, the combination of KGN and TD was hereby chosen to investigate the potential chondrogenic differentiation of MSCs. Various concentrations of TD were tested to determine the ideal dose to induce chondrocyte differentiation when combined with KGN. The results showed that when coupled with >10 nM TD, the clear deposition of cartilaginous matrices was observed with Toluidine blue and Safranin O staining, comparing with 100 nM KGN alone, suggesting that the cultures were augmented with TD, and the peak was at 100 nM. In contrast, the concentrations of TD exceeding 100 nM inhibited chondrogenesis (Fig. 3A). Therefore, the combination of 100 nM TD plus 100 nM KGN was chosen to obtain significant chondrogenesis of MSCs. The strong ability of TD and KGN on chondrogenesis was also assayed by immunofluorescence (CBFβ)-FISH (RUNX1) staining. As shown in Fig. 3B, the expression of RUNX1 mRNA and CBFβ in the cytoplasm was both upregulated in TD + KGN group, compared to the other three groups. Meanwhile, the level of related genes on chondrogenesis at seven days was analyzed through qPCR (Fig. 4A). The results revealed that the mRNA level of RUNX1was also elevated by the induction of TD, and that it was not further up-regulated by the co-treatment of KGN, which were fully consistent with the previous results. Moreover,the upregulation of cartilage-specific genes (*SOX9*, *Acan*, *Col II*) was notably enhanced when KGN was combined with TD, in comparison to cells treated with KGN or TD individually. The hypertrophy gene (*Col X* expression) of chondrogenesis was also examined, and no difference was detected between the groups. These results demonstrated the synergistic effects of KGN and TD on the enhanced chondrogenesis of MSCs without affecting hypertrophy.

Western blotting was used to analyze the levels of related proteins at seven days. Compared with the control group, the treatment with KGN, TD, or the combination of KGN and TD significantly increased the expression levels of transcription factors RUNX1 and SOX9. It was found that the combined treatment of KGN and TD led to significantly higher expression levels of SOX9 and RUNX1 than those from treatment with either KGN or TD alone (Fig. 4B–C). Previous studies have provided no evidence supporting that KGN upregulates RUNX1 expression through transcriptional activation. However, our current findings demonstrate that KGN enhances RUNX1 protein levels through a post-transcriptional mechanism, specifically by promoting the translational efficiency of RUNX1 mRNA rather than modulating its transcriptional activity. As a result, the expression of ACAN and Col II, which are the downstream target genes of SOX9 and RUNX1, also changed in a similar manner at seven days. There was no significant difference in the expression levels of Col X, which causes the formation of fibrocartilage in vivo, between the KGN + TD group and the other three groups (Fig. 4D–E). To further confirm the chondrogenic differentiation of MSCs, the cells were subjected to immunostaining for the expression of RUNX1, ACAN, and COL II proteins after induction. Among all the experimental groups, the control group had the lowest fluorescence signal. This indicates that MSCs do not undergo chondrogenesis without external cytokines. The group induced by KGN had a staining pattern similar to that of the group induced by TD. The group induced by both KGN and TD had increased staining compared with both single-induced groups (Fig. 4F–G). In brief, KGN alone is not enough to effectively form cartilage-related proteins. The combination of KGN and TD shows a promising strategy for application in cartilage tissue engineering through RUNX1 regulation.

3.4. Preparation and characterization of liposomes and hydrogels

The liposome nanocomposite, which serves as an outstanding bioactive delivery carrier, has been extensively utilized in controllable delivery systems as well as tissue regeneration [32,37]. In the present study, both KGN and TD are hydrophobic substances. They are encapsulated within liposomes through the thin film hydration method to enhance their loading and delivery efficiency and to ensure their uniform distribution within hydrogels. To verify the successful preparation of the liposomes, the sizes of the synthesized liposomes loaded with KGN (KGN@Lipo) and TD (TD@Lipo) were determined by DLS. The results demonstrated that the size distribution was around 294.8 ± 46.3 nm for KGN@Lipo and 312.1 ± 48.2 nm for TD@Lipo. Additionally, the morphology and size of the synthesized liposomes were further confirmed by TEM, which showed a uniform spherical shape with a diameter of approximately 300 nm (Fig. 5A–B). GelMA hydrogels were prepared containing various concentrations of 1:1 ratio of KGN@Lipo and TD@Lipo (0–1000 nM) to verify the synergistic effect of KGN and TD on chondrogenesis. MSCs were grown on the hydrogels for seven days and subsequently stained using Safranin O and Toluidine blue. These results revealed that the 500 nM concentration group exhibited higher cartilage matrix synthesis following induction. Additionally, the KGN + TD@ GelMA resulted in stronger staining of Safranin O and Toluidine blue than KGN@GelMA or TD@GelMA for cells on hydrogels (Fig. S5). Furthermore, macroscopic observation revealed that the KGN@GelMA hydrogel was milky white, while the TD@GelMA and TD + KGN@GelMA hydrogel was creamy yellow due to the addition of TD-loaded liposomes. The hydrogel microscopic structures were viewed using SEM. All hydrogels exhibited uniform-sized pores, with similar pore sizes in different groups (Fig. 5C–D). The swelling properties of hydrogels were also tested, showing that the swelling ratios were also similar in different groups (Fig. 5E). Next, the estimation of the release of KGN and TD from the composite hydrogel was carried out. The KGN@lipo and TD@lipo can be released from GelMA slowly for nearly 30 days, without a burst release at the early stage in vitro (Fig. 5F). The findings suggested that the presence of liposomes had no impact on the overall structure-property of GelMA. Following an 50-day degradation

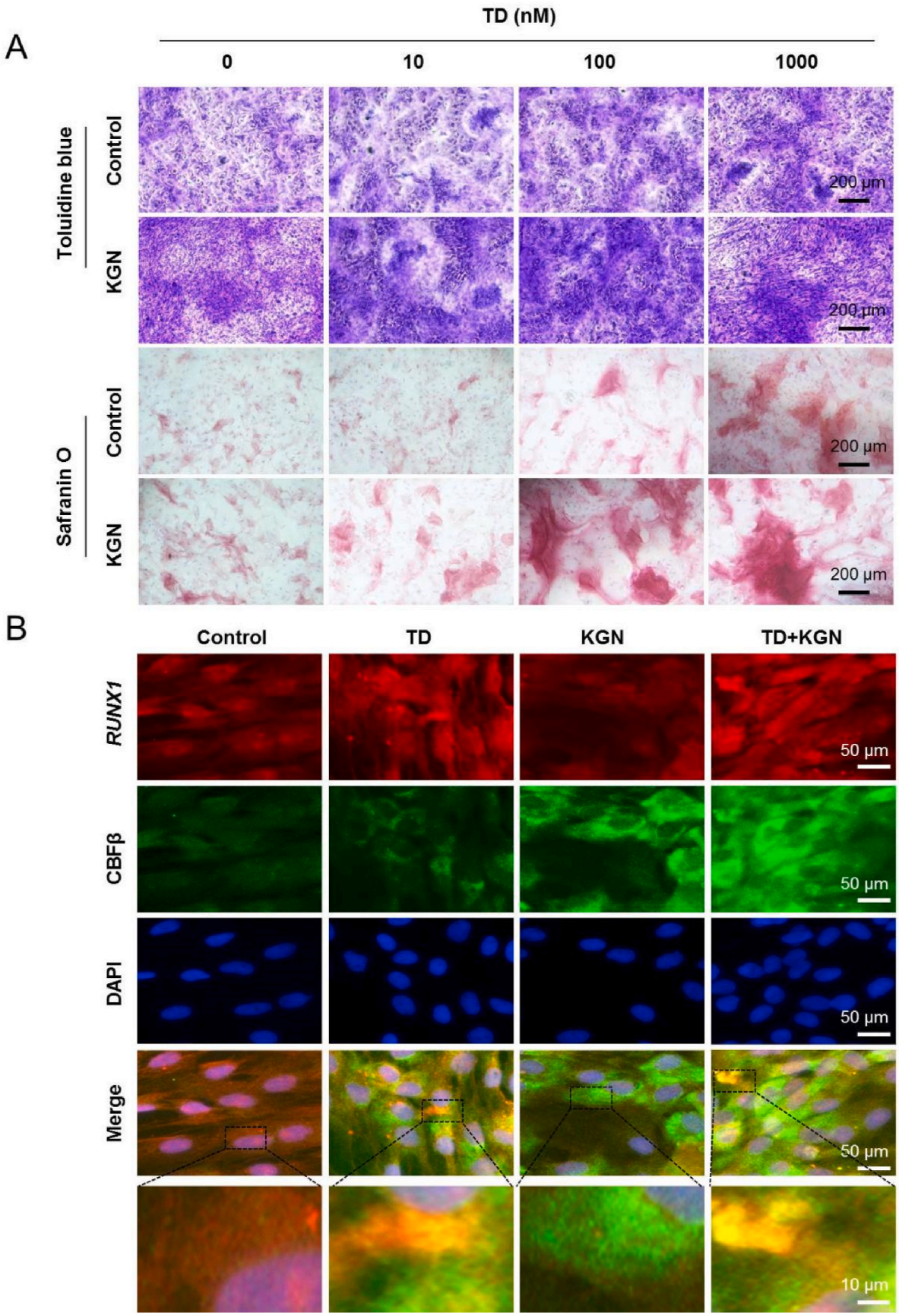

Fig. 3. Synergistic effects of KGN and TD on chondrogenesis of MSCs. **A** Toluidine blue and Safranin O staining in 24-well plates cultured with KGN and various concentrations of TD for seven days. Scale bar: 200 μm. **B** Double staining for IF (CBFβ)-fluorescence in situ hybridization (FISH) (RUNX1) in MSCs with the treatment of KGN or/and TD for 24 h. Scale bar: 50 μm.

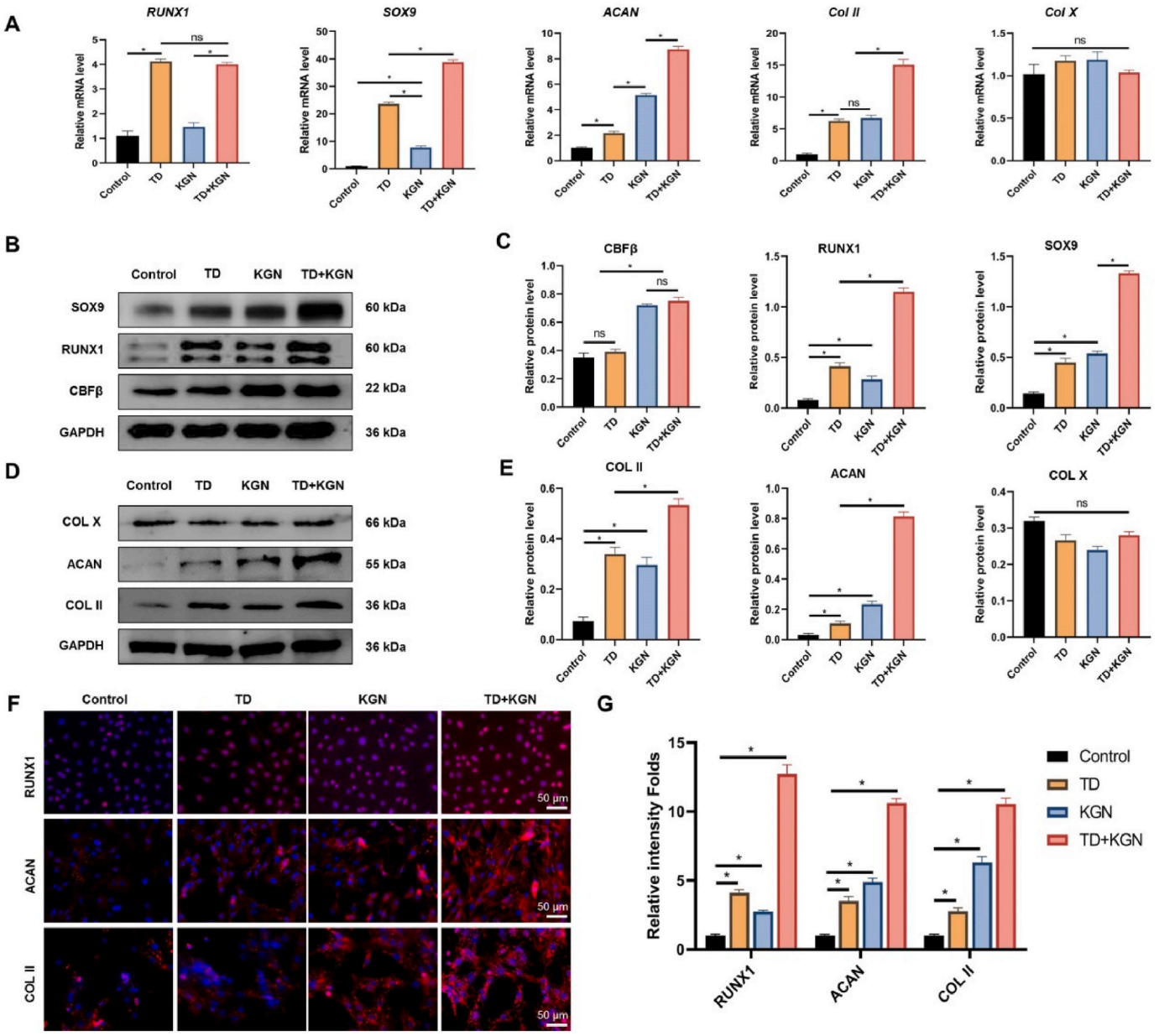

Fig. 4. Analysis of MSCs in different treatments using Western blot and immune-fluorescence techniques. (**A**) Gene expression analysis, including *Runx1, Sox9, Acan, Col II,* and *Col X* of MSCs after culturing for 7 days. (**B-E**) Protein levels of CBFβ, RUNX1, SOX9, Col II, ACAN, and Col X on the day 7 were determined by western blot. The levels of indicated proteins were quantified by Image J and normalized to GAPDH. (**F-G**) The immuno-staining and quantitative analysis of chondrocyte marker proteins (RUNX1, ACAN, COL II) in the induced cells, Scale bar: 100 μm. (n = 3, *: $p < 0.05$; ns: no significant difference).

period in vitro, the hydrogel scaffolds demonstrated degradation rates was less than 80 %, which sustained a prolonged release of KGN@lipo and TD@lipo (Fig. 5G).

In tissue engineering, the biocompatibility of liposome hydrogels plays a crucial role in maintaining cell viability, promoting cell proliferation, and facilitating cell differentiation. To assess the biocompatibility of the hydrogels, MSCs were cultured on their surfaces for three days. Subsequently, the cytoskeleton of the MSCs was stained with phalloidin. It was observed that the MSCs spread well on all of the hydrogels, and no differences were detected among each group (Fig. S6A). In this study, the cell viability on the liposome hydrogel was also examined using the CCK-8 assay. MSCs were seeded onto different types of hydrogels for one, three, and five days. The OD value, which indicates cell viability, increased gradually with the prolongation of the culture time, demonstrating that the proliferation of MSCs also increased gradually. Moreover, there was no significant difference in cell viability among the various groups, implying that the application of liposomes did not exert any adverse impacts on the cells (Fig. S6B). As revealed by the live/dead assay (Fig. S6C), nearly all cells were stained with green fluorescence, while the red fluorescence was scarcely visible from three days in the different hydrogels. This indicates the excellent biocompatibility of the liposome hydrogels. Consequently, these results show that liposome hydrogels possess remarkable biocompatibility and can enhance the proliferation of MSCs.

3.5. *The "EVs-in-ECM" mimicking system promotes in-situ cartilage regeneration in vivo*

For the in vivo experiments, a cartilage defect was created on the trochlear groove of male Sprague - Dawley rats using the modified corneal trephine. The cartilage regeneration capabilities of different groups, namely the defect group (receiving no treatment), GelMA group,

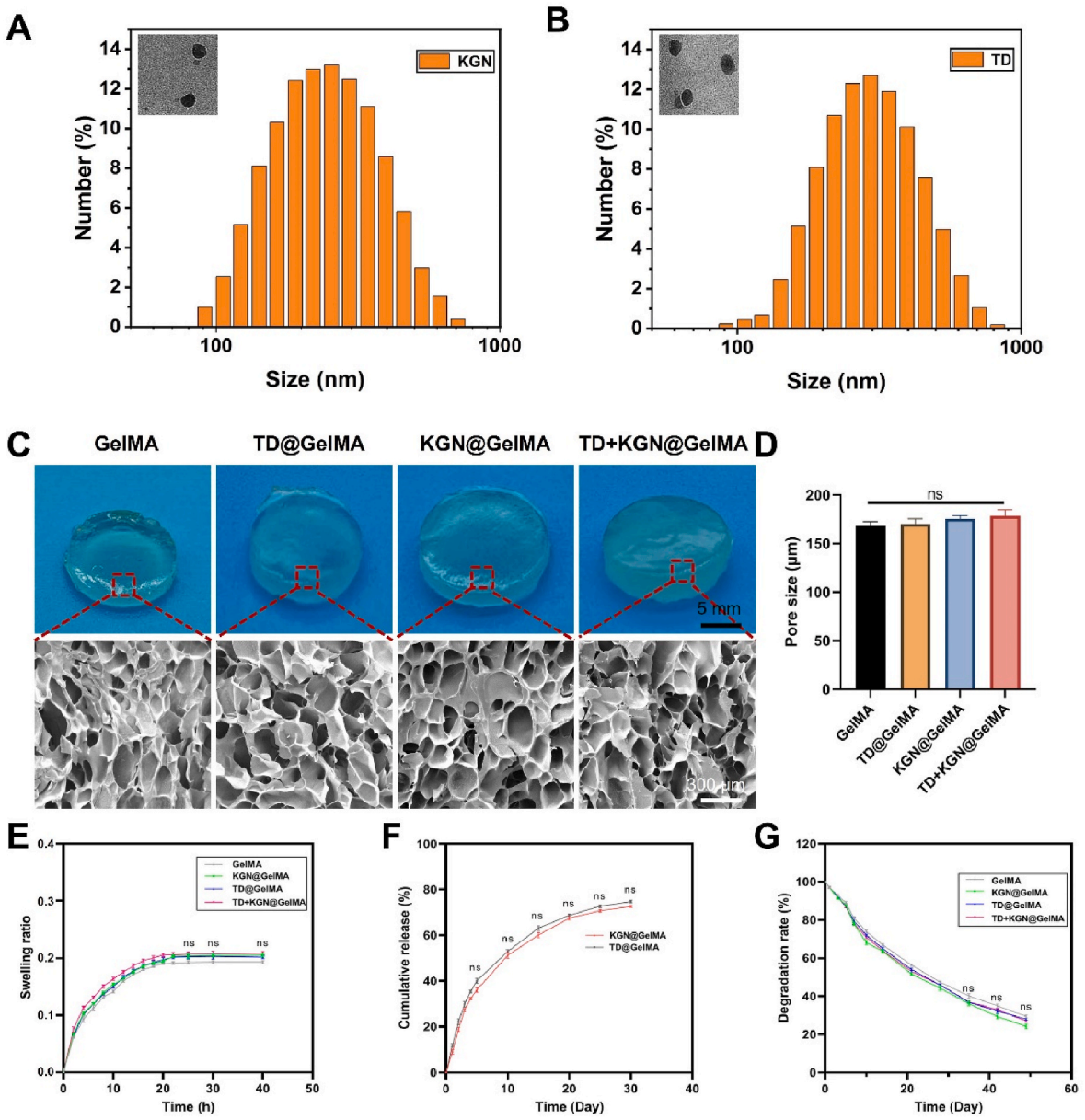

Fig. 5. Preparation and characterization of liposomes and hydrogels **A** The particle size and TEM images of KGN@Lipo **B** The particle size and TEM images of TD@Lipo **C** Gross morphology and SEM images of hydrogels. Scale bar: up, 5 mm; down, 300 μm. **D** Pore sizes of hydrogels. **E** Swelling behaviors of hydrogels. **F** Cumulative release of KGN@lipo and TD@lipo from GelMA hydrogels at each time point. **G** The degradation of hydrogels. (n = 3, *: $p < 0.05$; ns: no significant difference).

KGN@GelMA group, TD@GelMA group, and KGN + TD@GelMA group, were evaluated in a cartilage defect model at six and twelve weeks. At six weeks, although defects remained in all groups, the defects in the KGN@GelMA, TD@GelMA, and KGN + TD@GelMA groups started to be covered with a certain amount of white, cartilage-like tissue. In contrast, the defects in the untreated defect group and GelMA group were only filled with reddish tissue. When the treatment period was extended to twelve weeks, the KGN + TD@GelMA group presented a smooth surface similar to that of the normal group, and the boundary of the newly formed tissue was well integrated with the surrounding cartilage.The KGN@GelMA and TD@GelMA groups formed just a small amount regeneration of organized hyaline cartilage in the defective area of the patellar grooves and clearly demarcated from surrounding tissue at twelve weeks after surgery. However, for the defect and GelMA groups, the defected site was only filled with fibrous tissue and osteophytes appeared in areas of normal cartilage (Fig. 6A). Moreover, the ICRS cartilage repair macroscopic score revealed a significantly superior repair outcome in the KGN + TD@GelMA groups compared to the other groups, approaching the level of the sham group twelve weeks after implantation (Fig. 6B). Meanwhile, μ-CT imaging revealed that the subchondral bone defect was filled with newly regenerated bone tissue and the surface of the bone was completed in the KGN + TD@GelMA group. In contrast, fewer newly formed bones were observed around the border of the subchondral bone defect in other groups, with the center of the defect remaining empty (Fig. 6C). Based on the μ-CT imaging results, several bone parameters, such as BVF, Tb.Th, and BMD (Figs. S7A–C), underwent changes with time and treatment intervention. Compared to the normal group, the defect group exhibited a significant decline in the BVF, Tb.Th, and BMD both at six weeks and twelve weeks. However, following the treatment with KGN + TD@GelMA, the bone parameters were improved and approached the normal level. No statistical difference was detected between the KGN + TD@GelMA group and normal

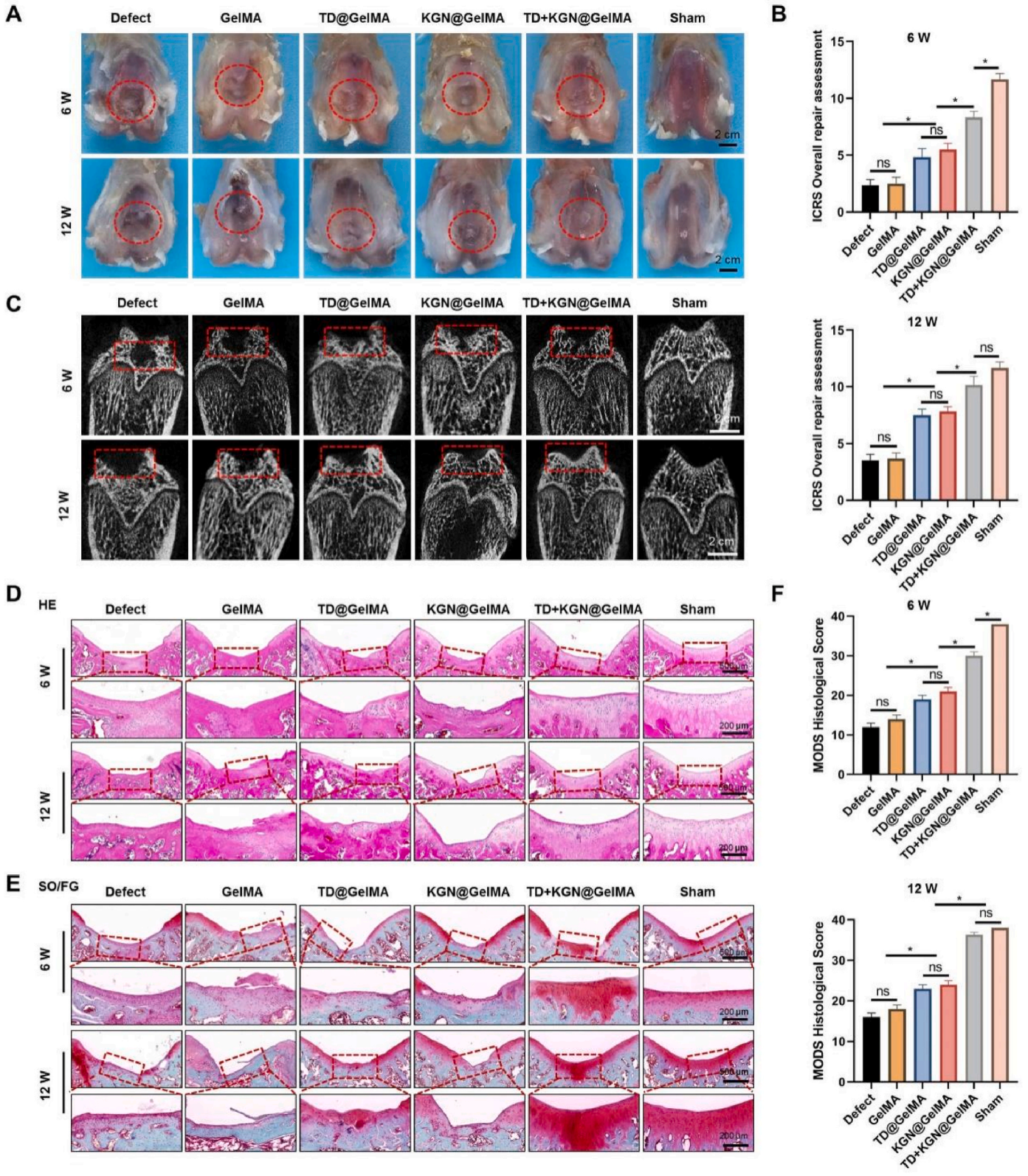

Fig. 6. Cartilage repair efficacy in vivo. **A** Macroscopic appearances of cartilage repair were observed at six and twelve weeks following the creation of 2 mm defects. **B** The ICRS macroscopic scores of the repaired cartilages were evaluated at six and twelve weeks. **C** μ-CT scans. The red rectangles show the defect sites of the subchondral bone, scale bar, 2 mm. **D** HE staining. **E** SO/FG staining. **F** The MODS histological score was utilized to assess the extent of cartilage healing. Scale bars: down (enlarged area), 200 μm; up, 500 μm. (n = 3, *: $p < 0.05$; ns: no significant difference).

group at twelve weeks. Moreover, KGN + TD@GelMA exhibited a notably higher recovery level compared to KGN@GelMA and TD@GelMA, indicating superior restoration of subchondral bone with increased bone content. In summary, the combination of KGN and TD exerted favorable subchondral bone repair effects.

The histomorphological staining technique was employed to demonstrate the types of repaired tissues resulting from different treatment methods. The structure of regenerated bone tissues as well as the organization of chondrocytes was assessed through HE staining. In both the defect and GelMA groups, fibrous tissue filled the defect, resulting in joint surfaces that were rough and exhibited uneven density. In contrast, in the KGN + TD@GelMA group, there was significant recovery of the subchondral bone at six weeks, and as time progressed to twelve weeks, the defect disappeared and was structurally similar to the sham group. In the KGN@GelMA or TD@GelMA groups, a gap was still present between the newly formed tissue and the surrounding original tissue at twelve weeks. This clearly demonstrates that the combined action of KGN and TD was highly effective in promoting the repair of osteochondral defects (Fig. 6D). The results of SO/FG were similar to HE. The cartilage layer was reconstructed in the KGN + TD@GelMA group, with a thickness similar to the normal group and a smooth surface. However, for the TD@GelMA or KGN@GelMA groups, the cartilage at the defect failed to be restored to the same level as the adjacent normal cartilage layer, with thinner thickness, lighter Safranin O, and even localized concavity. For both the defect and GelMA groups, the effect was worse, with no significant cartilage repair observed until twelve weeks (Fig. 6E). Six weeks after the surgery, the KGN + TD@GelMA group showed an 8.3 % rise in the MODS histological scores when compared to the KGN@ GelMA group. Similarly, twelve weeks after the surgery, the KGN + TD@GelMA group demonstrated an anticipated improvement in its cartilage repair potential, which was manifested by a 13.2 % increase in the MODS histological scores in comparison with the control group (Fig. 6F).

Col II is the hyaline cartilage marker protein, which shows the cartilage matrix synthesis of chondrocytes. Immunohistochemical staining was carried out to assess the amount of Col II in the repaired tissue(Fig. 7A). The results showed that there was no clear positive staining present in either the defect group or the GelMA group at any time. For the TD@GelMA or KGN@GelMA groups, the expression of Col II in the defect area was higher compared to the defect or GelMA groups, yet it remained lower than the surrounding normal tissue. However, in the KGN + TD@GelMA group, the content of Col II increased at six weeks and further increased at twelve weeks, showing no significant disparities from the adjacent native cartilage. Moreover, the level of COL II of the KGN + TD@KGN group was notably raised by 18.3 % and 26.3 % at 6 and 12 weeks respectively, when compared with the KGN@GelMA group (Fig. 7B). The efficiency of inhibiting chondrocyte hypertrophy during the treatment process in vivo was investigated by evaluating the expression of Col X by immunohistochemical staining (Fig. 7C). The results further confirmed that KGN + TD@ GelMA enhanced chondrogenic differentiation without affecting hypertrophy. However, in the other surgical groups, there was varying upregulation in the expression of Col X, especially in the defect and GelMA groups. Additionally, the immunostaining examination of Col X revealed reduced expression in the KGN + TD@GelMA group (Fig. 7D). Furthermore, The expression of RUNX1 protein was consistent with the in-vitro experiments. In both the 6-weeks and 12-weeks, the RUNX1 expression in the KGN + TD@GelMA group was significantly higher than that in the KGN@GelMA group and the TD@GelMA group. (Fig. S8). These findings suggest that the combination of KGN and TD acts as a promoter of chondrogenic differentiation while inhibiting hypertrophy.

4. Discussion

Due to its lack of self-repair in chronic degenerative joint diseases like OA, cartilage is lost in an irreversible manner, which leads to an imbalance in its synthesis and accelerates its degradation [38,39]. Certain traumatic injuries reach the subchondral bone, which may trigger some intrinsic fibrocartilage repair response. However, this tissue has been demonstrated not to be a substitute for hyaline articular cartilage [40]. Furthermore, MSCs possess the capability to regenerate cartilage and differentiate into a range of other connective tissues [41]. It has been reported in the literature that KGN promotes MSC chondrogenesis and proliferation, but these effects are limited [16,30,42–44]. According to published research, KGN had little effect on chondrogenesis and nodule formation, whereas TGF-β stimulation could enhance the chondrogenesis in MSCs [30,42,45–47]. Previous studies have suggested that KGN induces chondrogenesis through enhancing the formation of CBFβ-RUNX1 dimer in nucleus [16]. However, in this study, RUNX1 was found to locate in nucleus whereas CBFβ was predominantly dispersed in cytoplasm. The translocation of CBFβ into nucleus was not observed after KGN treating. This finding were double confirmed by IF using different types of antibodies anti-CBFβ as well as western blot, and consistent with the present study that CBFβ dominantly located in cytoplasm for lacking nuclear localization sequence [17]. Therefore, understanding the molecular mechanisms of KGN is important to develop novel therapeutic approaches to promote chondrocyte differentiation.

Previous investigation has demonstrated that KGN is capable of regulating the expression of RUNX1 so as to prompting the chondrogenic differentiation of MSCs [3,48,49]. Obvious alterations in RUNX1 protein levels were hereby detected in MSCs after short-term treatment with KGN, but RUNX1 mRNA levels were stable. Fan et al. [15] suggest that KGN facilitates the chondrogenesis of MSCs by reducing the degradation of RUNX1. Other studies also found that CBFβ can endogenously make a complex with RUNX1 and protect RUNX1 from polyubiquitination-mediated proteasomal degradation [50–52]. However, the protein declination of RUNX1 was prolonged in the presence of CHX, which implies that KGN might not only regulate the stability of RUNX1 but also be involved in enhancing its expression. Co-IP assays were employed to confirm that during the process of chondrogenic differentiation of MSCs, translation initiation factor eIF4B was strongly bound to CBFβ to form a complex intervened by KGN. The experiment in FISH revealed that the CBFβ protein and RUNX1 mRNA are predominantly located in the cytoplasm, suggesting that CBFβ functions as a translation enhancer by binding to eIF4B to regulate the target RUNX1 mRNA in the cytoplasm. Furthermore, Malik et al. [17] also reported that RUNX1 mRNA is bound and translationally regulated by CBFβ. Together, these results support a model in which KGN regulates RUNX1 translation through CBFβ to accelerate cartilage regeneration and rehabilitation.

Members of the RUNX family, comprising RUNX1, RUNX2, and RUNX3, play crucial roles in the development of the skeletal system [53,54]. RUNX1 is a crucial transcription factor that is necessary for chondrogenesis and the suppression of hypertrophy [12,21,55,56]. The levels of CBFβ and RUNX1 decrease with aging and OA progression [57]. Aini et al. [58] showed that injecting RUNX1 mRNA intra-articularly resulted in increased expression of chondrogenic genes and reduced IL-1β levels in the articular cartilage of mouse with osteoarthritis. Tang et al. [55] discovered that the elimination of RUNX1 led to a decrease in the expression of SOX9, Ihh, Ptc, and CyclinD1, and also damaged the proliferative and hypertrophic zones within the growth plate, indicating that RUNX1 plays a central part in the proliferation of chondrocytes. In order to improve the expression of RUNX1, a new intervention method of the combined application of KGN and TD is hereby proposed. The target molecule of TD significantly enhances the expression of RUNX1 mRNA,a well-known chondrogenic factor [22]. It was verified that the rate of de-differentiated cells could re-differentiate into chondrocytes after TD treatment, which was demonstrated by the enhancement of various chondrogenic markers, such as the expression of Col II and GAG, as well as the results of alcian blue staining and toluidine blue staining.

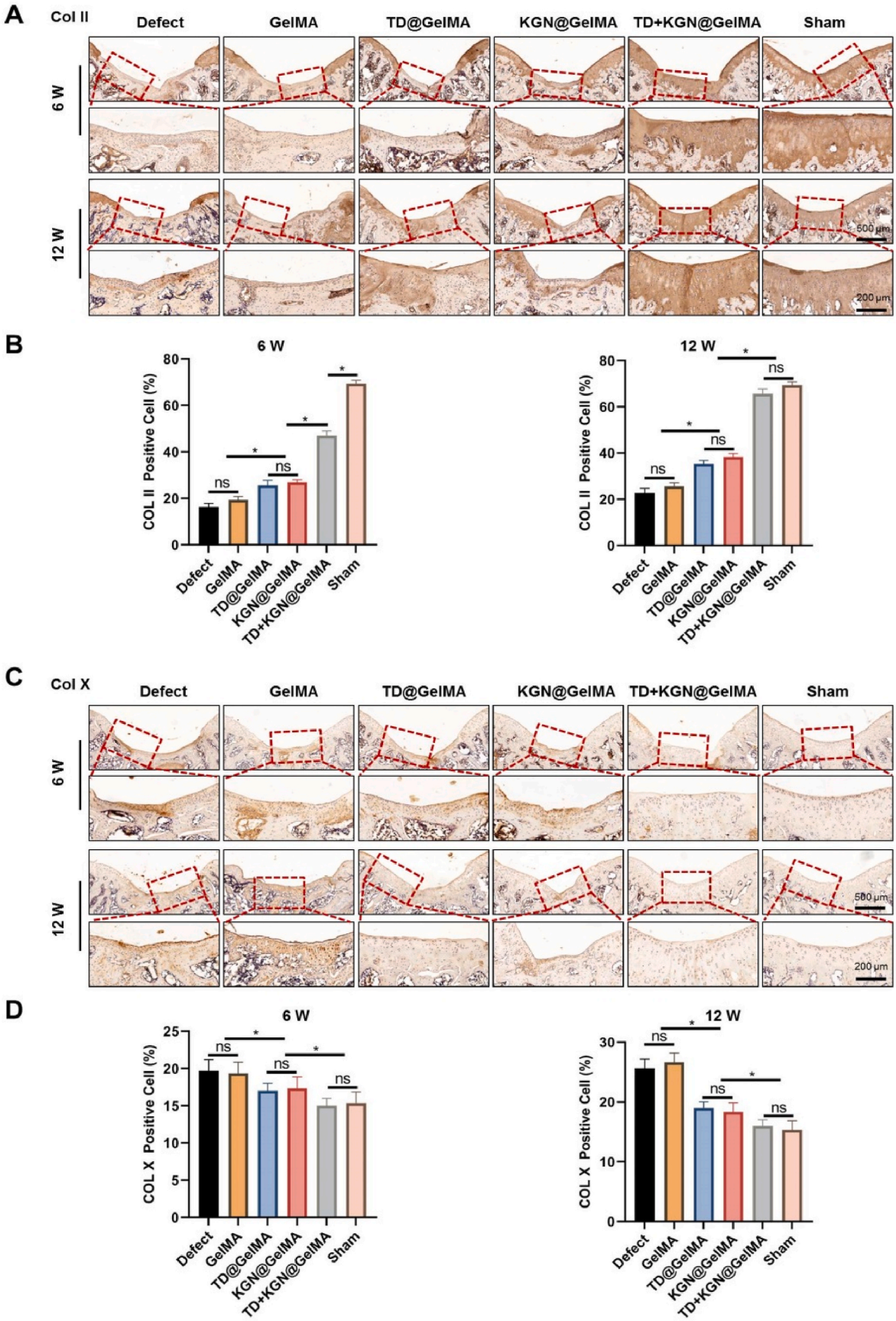

Fig. 7. The expression of matrix protein at six and twelve weeks post-surgery. **A** Immuno-histochemical staining of Col II in the articular cartilage. **B** Measuring the proportion of Col II-positive cells in the articular cartilage. **C** Immunohistochemical staining of Col X in the articular cartilage. **D** Quantifying the percentage of Col X-positive in the articular cartilage. Scale bars: down (enlarged area), 200 μm; up, 500 μm. (n = 3, *: $p < 0.05$; ns: no significant difference).

However, there was no enhancement in the expression of Col X or Col I [59]. The findings in this study indicate that KGN further up-regulates the expression of RUNX1 when cooperating with TD through orchestrating RUNX1 translation and transcription. Moreover, SOX9 is also highly expressed when KGN combined with TD. SOX9 is a predominant transcription factor that is of crucial importance for the chondrogenic differentiation and development from MSCs [60]. Yano et al. [21] identified that RUNX1 directly bound regulatory sequences of the promoters of SOX9, induced the SOX9 expression during chondrogenesis, and their downstream targets included ACAN and Col II at both mRNA level and protein level in vitro. Furthermore,SOX9 not only functions as a transcriptional activator for chondrogenesis but also serves as a transcriptional repressor for osteoblast differentiation and chondrocyte hypertrophy by inhibiting the osteoblast target genes [61]. By harvesting MSCs from the femur of the Sprague-Dawley rats and culturing with KGN and/or TD, the results showed that the KGN + TD treatment significantly upregulated the expression of cartilage related protein and genes, without affecting hypertrophy (Col X). The results of safranine O and toluidine blue staining also showed that the chondrogenic effect was stronger in the KGN + TD group than in the KGN or TD group alone. These results indicate that KGN + TD had a stronger synergistic effect than KGN in terms of enhancing chondrogenic differentiation via the activation of RUNX1.

Free KGN and TD is the hydrophobic small molecule, which will be cleared from the synovial fluid very quickly when injected into the joint cavity. Repeated joint cavity injections pose the risk of bleeding, infection, and exacerbation of inflammation. Therefore, it is necessary to delay the intra-articular residence time of KGN and TD by means of a drug-carrying slow-release system. Liposomes are particularly suitable for delivering hydrophobic drugs, with a 90 % higher drug loading rate for corticosteroid delivery [62]. Nanoscale carriers have the ability to penetrate the ECM and cell membranes, enabling direct drug release in the ECM or cells [63]. Due to their excellent biocompatibility and degradability, liposomes have been proposed as appropriate nano/-microparticles for transporting therapeutic agents. Up to now, numerous liposomal drug formulations have been commercialized and given approval in medical practice [64,65]. In this study, lecithin and cholesterol were used to encapsulate the drug to form liposomes aiming to enhance the stability of nanoparticles, alleviate burst release, and provide matrix for cell homing and regeneration, and GelMA was used as the final carrier to mix the liposomes. Due to its excellent biocompatibility, low immunity, adjustable mechanical properties, and abundant availability, GelMA has been widely used in cartilage repair [26,66,67]. At the same time, the porous structure of GelMA can provide space to contain and protect liposomes [68]. Both CCK-8 and live-dead staining results indicated that KGN@GelMA and TD@GelMA were not significantly cytotoxic. The relative literature reported that the slowed degradation of the GelMA further prolonged the release time of liposome drug [69,70]. The assay on release behavior indicated that both KGN and TD were continuously released from the GelMA hydrogel over a period of more than four weeks. Continuous drug delivery stimulates MSCs to undergo differentiation into cartilage tissue and facilitate the repair of damaged cartilage. The incorporation of KGN@Lipo and TD@Lipo into GelMA did not exert any significant influence on its mechanical characteristics and biocompatibility, enabling the scaffold to provide a comparable mechanical environment for the cells and encourage them to spread and grow well within the hydrogel. Consequently, an "EVs-in-ECM" mimicking system was capable of filling the cartilage defect and supplying the requisite mechanical support after being crosslinked, alleviating the degeneration process of articular cartilage.

Finally, to achieve in situ cartilage regeneration, the hydrogels can be implanted in knee cartilage defect sites in rats [71]. After implanting hydrogels into the defect site, the defects in the KGN + TD@GelMA group were nearly completely filled with regenerated tissue, while the defects in the other groups were just partially covered according to μ-CT, HE and SO/FG staining. The immunohistochemical imaging also showed intense staining for Col II in the KGN + TD@GelMA group, more effective than KGN@GelMA or TD@GelMA for promoting cartilage repair. Ono et al. [44] also reported that the efficiency of chondrogenesis induced by KGN alone is impeding its further clinical application. However, combining KGN with TGF-β3 or BMP-2 could induce chondrogenesis [47,72]. Though KGN and TD exhibited the capacity in promoting cartilage matrix synthesis and inhibiting chonodrocytes hypertropy compared to KGN + TD. However, the in vitro result displayed different effect. The combination of KGN and TD not only significant enhanced the formation of cartilage matrix but also prevented the expression of ColX. The different result might be derived from different culture condition in vitro and in vivo. In the in vitro study, MSCs were cultured in a chondrogenic induction medium with low concentration of serum, which was prone to promote chondrogenic differentiation but inhibit chondrocyte hypertrophy in all the groups including control, KGN, TD and KGN + TD. While in vivo, the complicated components in subchondral bone, the interference from other cells such as fibroblasts, and the possible inflammatory environment in defect might led to cartilage hypertrophy [30]. However, the combination of KGN and TD in “EVs-in-ECM” mimicking system obviously prevented the expression of Col X and showed superior effect on cartilage regeneration, hinting the necessity and potential of KGN and TD in cartilage repair. All of these results powerfully indicate the synergistic potential of KGN and TD in facilitating long-term cartilage regeneration. This is demonstrated by the fact that the defected bone tissues have been restored to the normal level in various aspects, such as the structure, morphology, composition and organization of bone tissues.

This research offers fresh perspectives on the mechanism of chondrocyte differentiation for KGN, which will contribute to the formulation of innovative approaches for treating cartilage injuries. Nevertheless, some limitations still remain to be addressed. First, this study only focused on a single RUNX1 target gene. CBFβ may control numerous target genes and modulate multiple signaling pathways. Therefore, further studies are needed to answer these questions. Second, the rat cartilage defect model was hereby used, in which the injured cartilage environment is quite different from the microenvironment of injury in daily human life [73]. Third, the biomechanical tests such as indentation testing, will be adopted to better verify the functions of the repaired cartilage. Furthermore, it is necessary to conduct studies using a large animal model with a long-term follow-up in order to verify its clinical potential in the future.

5. Conclusion

In this study, we demonstrate a novel mechanism in which KGN promotes the translation of RUNX1 mRNA through CBFβ binding with eIF4B. Based on this finding, we propose the strategy of efficiently chondrogenesis through an “EVs-in-ECM” mimicking system orchestrating RUNX1 transcription and translation. Finally, we demonstrated the in vivo effects through animal experiments, providing a new and convenient method for in-situ cartilage repair.

CRediT authorship contribution statement

Qi Cheng: Conceptualization. **Qianping Guo:** Data curation. **Xiaoyu Zhang:** Funding acquisition. **Yuanchen Zhu:** Methodology. **Chengyuan Liu:** Project administration. **Huan Wang:** Software. **Caihong Zhu:** Supervision. **Li Ni:** Formal analysis. **Bin Li:** Validation. **Huilin Yang:** Writing – original draft.

Founding

The authors are grateful to the funding support from the National Natural Science Foundation of China (82072424, 81871805, 81902248), the Postdoctoral Science Foundation of China

(2021M702393) and the Suzhou Science and Technology Bureau Project (SKY2022185).

Declaration of competing interest

The authors declare that they have no known competing financial interests or personal relationships that could have appeared to influence the work reported in this paper.

Appendix A. Supplementary data

Supplementary data to this article can be found online at https://doi.org/10.1016/j.mtbio.2025.101569.

Data availability

Data will be made available on request.

References

[1] J. Wang, F. Zhang, W.P. Tsang, C. Wan, C. Wu, Fabrication of injectable high strength hydrogel based on 4-arm star PEG for cartilage tissue engineering, Biomaterials 120 (2017) 11–21.
[2] J. Wu, Q. Chen, C. Deng, B. Xu, Z. Zhang, Y. Yang, et al., Exquisite design of injectable hydrogels in cartilage repair, Theranostics 10 (21) (2020) 9843–9864.
[3] D. Shi, X. Xu, Y. Ye, K. Song, Y. Cheng, J. Di, et al., Photo-cross-linked scaffold with kartogenin-encapsulated nanoparticles for cartilage regeneration, ACS Nano 10 (1) (2016) 1292–1299.
[4] Y. Zhang, T. Zuo, A. McVicar, H.L. Yang, Y.P. Li, W. Chen, Runx1 is a key regulator of articular cartilage homeostasis by orchestrating YAP, TGFβ, and Wnt signaling in articular cartilage formation and osteoarthritis, Bone Res. 10 (1) (2022) 63.
[5] C.Y. Tang, M. Wu, D. Zhao, D. Edwards, A. McVicar, Y. Luo, et al., Runx1 is a central regulator of osteogenesis for bone homeostasis by orchestrating BMP and WNT signaling pathways, PLoS Genet. 17 (1) (2021) e1009233.
[6] G. Zhai, J. Doré, P. Rahman, TGF-β signal transduction pathways and osteoarthritis, Rheumatol. Int. 35 (8) (2015) 1283–1292.
[7] M. Wu, G. Chen, Y.P. Li, TGF-β and BMP signaling in osteoblast, skeletal development, and bone formation, homeostasis and disease, Bone Res. 4 (2016) 16009.
[8] F. Yano, S. Ohba, Y. Murahashi, S. Tanaka, T. Saito, U.I. Chung, Runx1 contributes to articular cartilage maintenance by enhancement of cartilage matrix production and suppression of hypertrophic differentiation, Sci. Rep. 9 (1) (2019) 7666.
[9] A. Kimura, H. Inose, F. Yano, K. Fujita, T. Ikeda, S. Sato, et al., Runx1 and Runx2 cooperate during sternal morphogenesis, Development 137 (7) (2010) 1159–1167.
[10] D.Y. Soung, L. Talebian, C.J. Matheny, R. Guzzo, M.E. Speck, J.R. Lieberman, et al., Runx1 dose-dependently regulates endochondral ossification during skeletal development and fracture healing, J. Bone Miner. Res. 27 (7) (2012) 1585–1597.
[11] L.S.H. Chuang, Y. Ito, The multiple interactions of RUNX with the hippo-YAP pathway, Cells 10 (11) (2021) 10.
[12] C. Zhou, Y. Cui, Y. Yang, D. Guo, D. Zhang, Y. Fan, et al., Runx1 protects against the pathological progression of osteoarthritis, Bone Res. 9 (1) (2021) 50.
[13] X. Xu, D. Shi, Y. Shen, Z. Xu, J. Dai, D. Chen, et al., Full-thickness cartilage defects are repaired via a microfracture technique and intraarticular injection of the small-molecule compound kartogenin, Arthritis Res. Ther. 17 (1) (2015) 20.
[14] Y.R. Chen, X. Yan, F.Z. Yuan, L. Lin, S.J. Wang, J. Ye, et al., Kartogenin-conjugated double-network hydrogel combined with stem cell transplantation and tracing for cartilage repair, Adv. Sci. 9 (35) (2022) e2105571.
[15] W. Fan, L. Yuan, J. Li, Z. Wang, J. Chen, C. Guo, et al., Injectable double-crosslinked hydrogels with kartogenin-conjugated polyurethane nano-particles and transforming growth factor β3 for in-situ cartilage regeneration, Mater. Sci. Eng., C 110 (2020) 110705.
[16] K. Johnson, S. Zhu, M.S. Tremblay, J.N. Payette, J. Wang, L.C. Bouchez, et al., A stem cell-based approach to cartilage repair, Science 336 (6082) (2012) 717–721.
[17] N. Malik, H. Yan, N. Moshkovich, M. Palangat, H. Yang, V. Sanchez, et al., The transcription factor CBFB suppresses breast cancer through orchestrating translation and transcription, Nat. Commun. 10 (1) (2019) 2071.
[18] N. Yoshida, T. Ogata, K. Tanabe, S. Li, M. Nakazato, K. Kohu, et al., Filamin A-bound PEBP2β/CBFβ is retained in the cytoplasm and prevented from functioning as a partner of the Runx1 transcription factor, Mol. Cell Biol. 25 (3) (2005) 1003–1012.
[19] G. Huang, K. Shigesada, K. Ito, H.J. Wee, T. Yokomizo, Y. Ito, Dimerization with PEBP2β protects RUNX1/AML1 from ubiquitin-proteasome-mediated degradation, EMBO J. 20 (4) (2001) 723–733.
[20] N.D. Sen, F. Zhou, M.S. Harris, N.T. Ingolia, A.G. Hinnebusch, eIF4B stimulates translation of long mRNAs with structured 5' UTRs and low closed-loop potential but weak dependence on eIF4G, Proc. Natl. Acad. Sci. U.S.A. 113 (38) (2016) 10464–10472.
[21] F. Yano, H. Hojo, S. Ohba, A. Fukai, Y. Hosaka, T. Ikeda, et al., A novel disease-modifying osteoarthritis drug candidate targeting Runx1, Ann. Rheum. Dis. 72 (5) (2013) 748–753.
[22] F. Yano, S. Ohba, Y. Hosaka, T. Saito, U.I. Chung, Disease-modifying effects of TD-198946 on progressed osteoarthritis in a mouse model, Ann. Rheum. Dis. 73 (11) (2014) 2062–2064.
[23] Y. Liu, M.B. Chan-Park, A biomimetic hydrogel based on methacrylated dextran-graft-lysine and gelatin for 3D smooth muscle cell culture, Biomaterials 31 (6) (2010) 1158–1170.
[24] J. Malda, J. Boere, C.H. Van, P. Van, M.H. Wauben, Extracellular vesicles — new tool for joint repair and regeneration, Nat. Rev. Rheumatol. 12 (4) (2016) 243–249.
[25] A.G. Kurian, R.K. Singh, K.D. Patel, J.H. Lee, H.W. Kim, Multifunctional GelMA platforms with nanomaterials for advanced tissue therapeutics, Bioact. Mater. 8 (2022) 267–295.
[26] G. Jiang, S. Li, K. Yu, B. He, J. Hong, T. Xu, et al., A 3D-printed PRP-GelMA hydrogel promotes osteochondral regeneration through M2 macrophage polarization in a rabbit model, Acta Biomater. 128 (2021) 150–162.
[27] K. Zheng, X. Zheng, M. Yu, Y. He, D. Wu, BMSCs-seeded interpenetrating network GelMA/SF composite hydrogel for articular cartilage repair, J. Funct. Biomater. 14 (1) (2023) 39.
[28] D. Hawthorne, A. Pannala, S. Sandeman, A. Lloyd, Sustained and targeted delivery of hydrophilic drug compounds: a review of existing and novel technologies from bench to bedside, J. Drug Deliv. Sci. Technol. 78 (2) (2022) 103936.
[29] X. Xu, Y. Liang, X. Li, K. Ouyang, M. Wang, T. Cao, et al., Exosome-mediated delivery of kartogenin for chondrogenesis of synovial fluid-derived mesenchymal stem cells and cartilage regeneration, Biomaterials 269 (2021) 120539.
[30] G. Liu, Q. Guo, C. Liu, J. Bai, H. Wang, J. Li, et al., Cytomodulin-10 modified GelMA hydrogel with kartogenin for in-situ osteochondral regeneration, Acta Biomater. 169 (2023) 317–333.
[31] J.R. Yu, M. Janssen, B.J. Liang, H.C. Huang, J.P. Fisher, A liposome/gelatin methacrylate nanocomposite hydrogel system for delivery of stromal cell-derived factor-1α and stimulation of cell migration, Acta Biomater. 108 (2020) 67–76.
[32] S. Wu, H. Zhang, S. Wang, J. Sun, Y. Hu, H. Liu, et al., Ultrasound-triggered in situ gelation with ROS-controlled drug release for cartilage repair, Mater. Horiz. 10 (9) (2023) 3507–3522.
[33] D. Zuncheddu, E. Della Bella, D. Petta, C. Bärtschi, S. Häckel, M.C. Deml, et al., Effect of glucose depletion and fructose administration during chondrogenic commitment in human bone marrow-derived stem cells, Stem Cell Res. Ther. 13 (1) (2022) 533.
[34] J.T. Weitkamp, M. Wöltje, B. Nußpickel, F.N. Schmidt, D. Aibibu, A. Bayer, et al., Silk fiber- reinforced hyaluronic acid-based hydrogel for cartilage tissue engineering, Int. J. Mol. Sci. 22 (7) (2021) 3635.
[35] F. Gao, Z. Xu, Q. Liang, H. Li, L. Peng, M. Wu, et al., Osteochondral regeneration with 3D-printed biodegradable high-strength supramolecular polymer reinforced-gelatin hydrogel scaffolds, Adv. Sci. 6 (15) (2019) 1900867.
[36] M.P. Van den Borne, N.J. Raijmakers, J. Vanlauwe, J. Victor, S.N. de Jong, J. Bellemans, International cartilage repair society (ICRS) and oswestry macroscopic cartilage evaluation scores validated for use in autologous chondrocyte implantation (ACI) and microfracture, Osteoarthr. Cartil. 15 (12) (2007) 1397–1402.
[37] H.S. O'Neill, C.C. Herron, C.L. Hastings, R. Deckers, A. Lopez Noriega, H.M. Kelly, et al., A stimuli responsive liposome loaded hydrogel provides flexible on-demand release of therapeutic agents, Acta Biomater. 48 (2017) 110–119.
[38] S. Jahn, J. Seror, J. Klein, Lubrication of articular cartilage, Annu. Rev. Biomed. Eng. 18 (2016) 235–258.
[39] C.D. DiDomenico, M. Lintz, L.J. Bonassar, Molecular transport in articular cartilage-what have we learned from the past 50 years? Nat. Rev. Rheumatol. 14 (7) (2018) 393–403.
[40] J.E. Bekkers, L.B. Creemers, A.I. Tsuchida, M.H. van Rijen, R.J. Custers, W.J. Dhert, et al., One-stage focal cartilage defect treatment with bone marrow mononuclear cells and chondrocytes leads to better macroscopic cartilage regeneration compared to microfracture in goats, Osteoarthr. Cartil. 21 (7) (2013) 950–956.
[41] F. Barry, M. Murphy, Mesenchymal stem cells in joint disease and repair, Nat. Rev. Rheumatol. 9 (10) (2013) 584–594.
[42] H. Jing, X. Zhang, M. Gao, K. Luo, W. Fu, M. Yin, et al., Kartogenin preconditioning commits mesenchymal stem cells to a precartilaginous stage with enhanced chondrogenic potential by modulating JNK and β-catenin-related pathways, FASEB J. 33 (4) (2019) 5641–5653.
[43] M. Hou, Y. Zhang, X. Zhou, T. Liu, H. Yang, X. Chen, et al., Kartogenin prevents cartilage degradation and alleviates osteoarthritis progression in mice via the miR-146a/NRF2 axis, Cell Death Dis. 12 (5) (2021) 483.
[44] Y. Ono, S. Ishizuka, C.B. Knudson, W. Knudson, Chondroprotective effect of kartogenin on CD44-mediated functions in articular cartilage and chondrocytes, Cartilage 5 (3) (2014) 172–180.
[45] R.S. Decker, E. Koyama, M. Enomoto-Iwamoto, P. Maye, D. Rowe, S. Zhu, et al., Mouse limb skeletal growth and synovial joint development are coordinately enhanced by Kartogenin, Dev. Biol. 395 (2) (2014) 255–267.
[46] Y. Zhao, B. Teng, X. Sun, Y. Dong, S. Wang, Y. Hu, et al., Synergistic effects of kartogenin and transforming growth factor-β3 on chondrogenesis of human umbilical cord mesenchymal stem cells in vitro, Orthop. Surg. 12 (3) (2020) 938–945.
[47] C. Liu, X. Ma, T. Li, Q. Zhang, Kartogenin, transforming growth factor-β1 and bone morphogenetic protein-7 coordinately enhance lubricin accumulation in bone-derived mesenchymal stem cells, Cell Biol. Int. 39 (9) (2015) 1026–1035.

[48] J. Wang, J. Zhou, N. Zhang, X. Zhang, Q. Li, A heterocyclic molecule kartogenin induces collagen synthesis of human dermal fibroblasts by activating the smad4/smad5 pathway, Biochem. Biophys. Res. Commun. 450 (1) (2014) 568–574.
[49] P. Chen, X. Liao, Kartogenin delivery systems for biomedical therapeutics and regenerative medicine, Drug Deliv. 30 (1) (2023) 2254519.
[50] X. Che, X. Jin, N.R. Park, H.J. Kim, H.S. Kyung, H.J. Kim, et al., Cbfβ is a novel modulator against osteoarthritis by maintaining articular cartilage homeostasis through TGF-β signaling, Cells 12 (7) (2023) 1064.
[51] X. Qin, Q. Jiang, Y. Matsuo, T. Kawane, H. Komori, T. Moriishi, et al., Cbfβ regulates bone development by stabilizing Runx family proteins, J. Bone Miner. Res. 30 (4) (2015) 706–714.
[52] N.R. Park, K.E. Lim, M.S. Han, X. Che, C.Y. Park, J.E. Kim, Core binding factor β plays a critical role during chondrocyte differentiation, J. Cell. Physiol. 231 (1) (2016) 162–171.
[53] M. Wu, C. Li, G. Zhu, Y. Wang, J. Jules, Y. Lu, et al., Deletion of core-binding factor β (Cbfβ) in mesenchymal progenitor cells provides new insights into Cbfβ/Runxs complex function in cartilage and bone development, Bone 65 (2014) 49–59.
[54] Y.J. Kang, J.I. Yoo, K.W. Baek, Differential gene expression profile by RNA sequencing study of elderly osteoporotic hip fracture patients with sarcopenia, J Orthop Translat 29 (2021) 10–18.
[55] J. Tang, J. Xie, W. Chen, C. Tang, J. Wu, Y. Wang, et al., Runt-related transcription factor 1 is required for murine osteoblast differentiation and bone formation, J. Biol. Chem. 295 (33) (2020) 11669–11681.
[56] F.J. Blanco, C. Ruiz-Romero, New targets for disease modifying osteoarthritis drugs: chondrogenesis and Runx1, Ann. Rheum. Dis. 72 (5) (2013) 631–634.
[57] H. Ding, X. Mei, L. Li, P. Fang, T. Guo, J. Zhao, RUNX1 ameliorates rheumatoid arthritis progression through epigenetic inhibition of LRRC15, Mol. Cells 46 (4) (2023) 231–244.
[58] H. Aini, K. Itaka, A. Fujisawa, H. Uchida, S. Uchida, S. Fukushima, et al., Messenger RNA delivery of a cartilage-anabolic transcription factor as a disease-modifying strategy for osteoarthritis treatment, Sci. Rep. 6 (2016) 18743.
[59] F. Yano, H. Hojo, S. Ohba, T. Saito, M. Honnami, M. Mochizuki, et al., Cell-sheet technology combined with a thienoindazole derivative small compound TD-198946 for cartilage regeneration, Biomaterials 34 (22) (2013) 5581–5587.
[60] A. Haseeb, R. Kc, M. Angelozzi, C. De Charleroy, D. Rux, R.J. Tower, et al., SOX9 keeps growth plates and articular cartilage healthy by inhibiting chondrocyte dedifferentiation/osteoblastic redifferentiation, Proc. Natl. Acad. Sci. U.S.A. 118 (8) (2021) e2019152118.
[61] G. Zhou, Q. Zheng, F. Engin, E. Munivez, Y. Chen, E. Sebald, et al., Dominance of SOX9 function over RUNX2 during skeletogenesis, Proc. Natl. Acad. Sci. U.S.A. 103 (50) (2006) 19004–19009.
[62] L. Cipollaro, P. Trucillo, N.L. Bragazzi, G. Della Porta, E. Reverchon, N. Maffulli, Liposomes for intra-articular analgesic drug delivery in orthopedics: state-of-art and future perspectives insights from a systematic mini-review of the literature, Medicina 56 (9) (2020) 423.
[63] F. Zhao, Y. Zhao, Y. Liu, X. Chang, C. Chen, Y. Zhao, Cellular uptake, intracellular trafficking, and cytotoxicity of nanomaterials, Small 7 (10) (2011) 1322–1337.
[64] J. Li, J. Ma, Q. Feng, E. Xie, Q. Meng, W. Shu, et al., Building osteogenic microenvironments with a double-network composite hydrogel for bone repair, Research 6 (2023) 21.
[65] F. Jahanmard, A. Khodaei, J. Flapper, O. Dogan, K. Roohi, P. Taheri, et al., Osteoimmuno- modulatory GelMA/liposome coatings to promote bone regeneration of orthopedic implants, J. Contr. Release 358 (2023) 667–680.
[66] X. Li, X. Li, J. Yang, Y. Du, L. Chen, G. Zhao, et al., In situ sustained macrophage-targeted nanomicelle–hydrogel microspheres for inhibiting osteoarthritis, Research 6 (2023) 131.
[67] B. Huang, P. Li, M. Chen, L. Peng, X. Luo, G. Tian, et al., Hydrogel composite scaffolds achieve recruitment and chondrogenesis in cartilage tissue engineering applications, J Nanobio- technology 20 (1) (2022) 25.
[68] D. Cao, X. Zhang, M.D. Akabar, Y. Luo, H. Wu, X. Ke, et al., Liposomal doxorubicin loaded PLGA-PEG-PLGA based thermogel for sustained local drug delivery for the treatment of breast cancer, Artif. Cells, Nanomed. Biotechnol. 47 (1) (2019) 181–191.
[69] Y. Liu, J. Du, P. Peng, R. Cheng, J. Lin, C. Xu, et al., Regulation of the inflammatory cycle by a controllable release hydrogel for eliminating postoperative inflammation after discectomy, Bioact. Mater. 6 (1) (2021) 146–157.
[70] X. Tian, Y. Zhang, L. Shen, G. Pan, H. Yang, Z. Jiang, et al., Kartogenin-enhanced dynamic hydrogel ameliorates intervertebral disc degeneration via restoration of local redox homeostasis, J Orthop Translat 42 (2023) 15–30.
[71] Y. Wang, Y. Chen, Y. Wei, Osteoarthritis animal models for biomaterial-assisted osteochondral regeneration, Biomater transl 3 (4) (2022) 264–279.
[72] Z. Jia, S. Wang, Y. Liang, Q. Liu, Combination of kartogenin and transforming growth factor-β3 supports synovial fluid-derived mesenchymal stem cell-based cartilage regeneration, Am J Transl Res 11 (4) (2019) 2056–2069.
[73] M. Tamaddon, H. Gilja, L. Wang, J.M. Oliveira, X. Sun, R. Tan, et al., Osteochondral scaffolds for early treatment of cartilage defects in osteoarthritic joints: from bench to clinic, Biomater transl 1 (1) (2020) 3–17.